Master's Theses and Capstones   Student Scholarship

Fall 2011

Synthesis of cadmium selenide-gold hybrid nanorods

Xiaoxiong Jia
University of New Hampshire, Durham

Follow this and additional works at: https://scholars.unh.edu/thesis

SYNTHESIS OF CADMIUM SELENIDE-GOLD HYBRID NANORODS

BY

XIAOXIONG JIA

B.S., China University of Petroleum, Beijing, 2009

THESIS

Submitted to the University of New Hampshire
in Partial Fulfillment of
the Requirements for the Degree of

Master of Science

in

Chemical Engineering

September, 2011

UMI Number: 1504952

UMI®

Dissertation Publishing

ProQuest®

This thesis has been examined and approved.

_____

Thesis Director, Dr. Xiaowei Teng,
Assistant Professor of Chemical Engineering

_____

Dr. Nivedita Gupta
Associate Professor of Chemical Engineering

_____

Dr. Gonghu Li,
Assistant Professor of Chemistry

_____

Date

Dedication

To my parents.

Acknowledgements

I would especially like to thank my advisor, Dr. Xiaowei Teng for sharing his enthusiasm and knowledge. His advice and counsel have been instrumental in the completion of the work.

I would also like to thank Dr. Nivedita Gupta and Dr. Gonghu Li for their help as committee members.
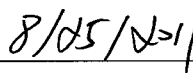
Thanks are also given to Nancy Cherim for her help with the transmission electron microscopy and energy dispersive spectroscopy equipments, John Newell for his assistant of laboratory troubleshooting, the writing center at University of New Hampshire for proofreading my thesis, and Wenxin Du for his assistant with the experiments.

TABLE OF CONTENTS

LIST OF TABLES

LIST OF FIGURES

ABSTRACT

SYNTHESIS OF CADMIUM SELENIDE—GOLD HYBRID NANORODS

by

Xiaoxiong Jia

University of New Hampshire, September, 2011

In this work, we reported the synthesis of cadmium selenide-gold (CdSe-Au) hybrid nanorods. The growth substrates, CdSe nanorods, were synthesized using a simple mono-injection method. The growth models for CdSe with different morphologies were proposed, and validated by the experimental results. It can be briefly described as concentrated CdSe monomers were prone to forming isotropic CdSe nanoparticles; while diluted CdSe monomers were prone to forming anisotropic CdSe nanorods. The growth of Au nanoparticles on the surface of CdSe nanorods was achieved via galvanic replacement reactions between Au ions ($AuCl_3$) and CdSe nanorods at room temperature. By adjusting the reaction times, the sizes of Au nanoparticles could be tuned from 1.7 ± 0.6 nm to 2.4 ± 0.9 nm.

CHAPTER 1 INTRODUCTION

Semiconductor nanomaterial have remarkable technological impacts on biomedical fluorescent labels, light emitting devices (LEDs), white-light laser sources, near-infrared emitters, solar cells, and tunable polarized lasers [1-6]. Among various semiconductors, diluted magnetic semiconductor (DMS) provides a possible solution to break the limits of modern electronic devices, such as limited packing density, high power consumption, or slow data processing speed. During the past two decades, research on developing new types of materials to serve as DMS has been intensively conducted [7-9]. Stable room-temperature ferromagnetism is considered as an essential prerequisite for DMS applications. However, many DMS nanostructures, such as (Ga, Mn)As and (In, Mn)As, are ferromagnetic only at low temperatures (< 110 K) [7, 27, 29]. A size-dependent magnetic property of gold (Au) nanoparticles has been reported recently [10-13], where Au nanoparticles with diameters less than 3 nm displayed ferromagnetism at 300 K, in contrast to diamagnetism found in its bulk counterpart. Therefore, the novel room-temperature ferromagnetism in Au nanoparticles may provide an alternative to design new type of DMS using Au nanoparticles as magnetic dopants.

1.1 Diluted Magnetic Semiconductor (DMS)

Magnetic storage materials, such as iron (III) oxide, cobalt and manganese-based alloys, have been extensively utilized for information recording purpose [7-9]. The most common magnetic storage devices include hard drives and magnetic tapes, which store information by manipulating the magnetizations in magnetic materials. During the past two decades, new kind of materials, DMS, have been brought to the research field. The

concept of DMS can be briefly described as the semiconductor materials with controllable ferromagnetic properties. These kinds of materials can be synthesized by introducing a small amount of magnetic dopants (spin carrier) to the semiconductor materials (**Figure 1.1**). By exploiting the state of spin in ferromagnetic materials, new functionalities for electronics and photonics can be derived if the ferromagnetism can be preserved above room temperature [19].
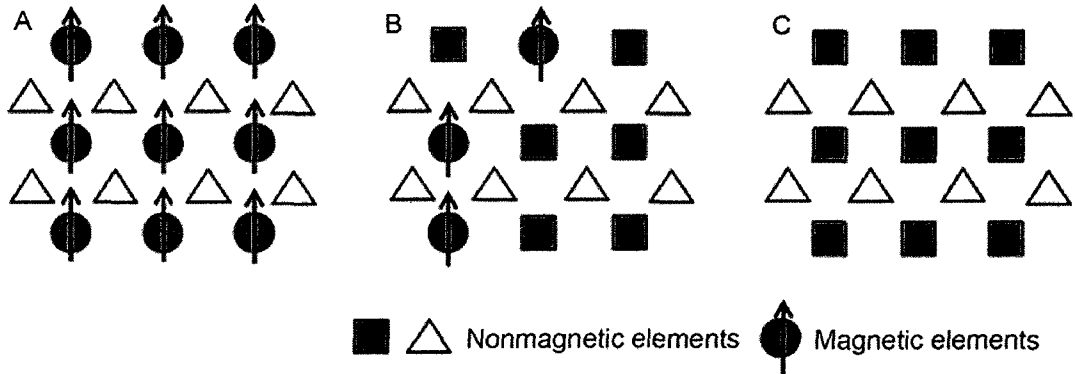
Figure 1.1 Three types of semiconductors: (**A**) a magnetic semiconductor, in which a periodic array of magnetic element is present; (**B**) a DMS between nonmagnetic semiconductor and magnetic element; and (**C**) a nonmagnetic semiconductor, which contains no magnetic ions.

The most common DMSs are III-V (for example, GaAs and InAs) and II-VI (for example, CdTe, ZnSe, CdSe and CdS) compounds with substituted transition metal ions (for example, Mn, Fe or Co). The utility of such materials depends on their ferromagnetism at room temperature; namely, their Curie temperatures should be above room temperature. Curie temperature is a critical point above which a ferromagnetic material becomes paramagnetic. For most DMSs, their Curie temperatures are in the range from 35 K to 110 K, which is far below room temperatures [8, 20-29].

The europium (Eu) chalcogenides are the most studied magnetic semiconductors in 1960s, of which the magnetism is from Eu^{2+}. The Curie temperatures of Eu chalcogenides are below 100 K, making this type of materials fail in the practical sense [8]. Since late 1990s, many research on DMS has been focusing on the III-V compounds (such as GaAs and InAs) with manganese (Mn) dopant [20-29], due to their marketing success in infra-red light-emitting diodes, high speed digital electronics (GaAs) and magnetic sensors (InAs) applications [7]. The (Ga, Mn)As [20-27] and (In, Mn)As [28,29] systems with ferromagnetic properties at low temperatures have been reported. Most of these materials were prepared by molecular beam epitaxy (MBE). For (In, Mn)As system, the highest Curie temperature reported is 35 K [29]; for (Ga,Mn)As system, the highest Curie temperature reported is 110 K [27]. Also, in some ternary alloys such as (In0.5Ga0.5)0.93Mn0.07As, the Curie temperature can also reach 110 K [7]. None of these materials exhibit stable ferromagnetism at room temperature. Alternative DMS with room-temperature ferromagnetism is highly demanded.

1.2 Magnetic Properties of Au Nanoparticles

In recent years, the study on ferromagnetism of Au nanoparticles has attracted special attentions [10-14]. People found that when the size of Au was less than 3 nm, it exhibited ferromagnetism at room temperature, in sharp contrast to its diamagnetism in bulk form. This unique room-temperature ferromagnetism makes Au nanoparticle a possible candidate to serve as the magnetic dopants in DMS.

Hori *et al.* studied the magnetic properties of alkaline thiol-capped Au nanoparticles with different sizes [10]. They found that 3 nm Au nanoparticles displayed the strongest magnetization at 1.8 K, while particles larger than 4 nm exhibited diamagnetism similar

to the bulk Au. In their subsequent work, using element-specific magnetization measurements, x-ray magnetic circular dichroism (XMCD) technique, they provided direct evidence that the ferromagnetism was an intrinsic property from Au, instead of possible magnetic impurities [11].

The Au atom has the electron configuration of $(4f)^{14}(5d)^{10}(6s)^1$. Due to s-p-d hybridization, a small amount of itinerant holes existing at the d band in bulk Au has been observed [12]. The corresponding hybridization resulted in the electron configuration as of $(4f)^{14}(5d)^{10-x}(6s)^{1+x}$. Thus, d-band holes can be generated in Au. When Au nanoparticles interact strongly with alkaline thiols, the number of d-band holes can further increases due to the charge transfer from Au site to thiols group [12]. The depleted d band is considered the origin of the ferromagnetism of Au in nanoscale at room temperature. An observation of d-charge depletion at the Au site and d-charge gain at the Pt site resulting in ferromagnetic Au/Pt alloys at room temperature was reported by Teng *et al.* [14]. Crespo *et al.* synthesized thiol-capped Au nanoparticles with 1.4 nm showing a clear ferromagnetism at 300 K [12, 13]. Both results indicate that nanoscale Au materials can preserve ferromagnetism at room temperature.

A serious of works about the growth of Au nanoparticles on cadmium selenide (CdSe), an II-VI semiconducting material, has been reported in the last decade [15-18]. The growth procedures of Au nanoparticles on CdSe have been well studied. Thus, CdSe is a suitable substrate material for measuring the room-temperature ferromagnetism of Au nanoparticles. In this work, we chose CdSe nanorods to achieve the growth of Au nanoparticles. In chapter 2, we present a simple method to produce different shaped CdSe systems. In chapter 3, we illustrate the approach to produce CdSe-Au hybrid nanorod

system. The sizes of Au nanoparticles on CdSe nanorod were successfully controlled by manipulating the reaction times. The synthesized CdSe-Au hybrid nanorods can be used to test the room-temperature magnetism of Au nanoparticles and the result may provide a scientific basis to the design of new types of DMS.

References:

1. Alivisatos, P. The use of nanocrystals in biological detection. *Nat Biotech* **22**, 47, (2004).

2. Coe, S., Woo, W.-K., Bawendi, M. & Bulović, V. Electroluminescence from single monolayers of nanocrystals in molecular organic devices. *Nature* **420**, 800-803 (2002).

3. V. I. Klimov et al., Optical gain and stimulated emission in nanocrystal quantum dots *Science* **290**, 314 (2000).

4. N. Tesster,V. Medvedev, M. Kazes, S. Kan, and U. Banin, Efficient near-infrared polymer nanocrystat light-emitting diodes, *Science* **295**, 1506 (2002).

5. W.U. Huynh, J. J. Dittmer, and A. P. Alivisatos, Hybrid nanorod-polymer solar cells *Science* **295**, 2425 (2002).

6. M. Kazes, D.Y. Lewis, Y. Ebenstein, T. Mokari and U. Banin, Lasing from semiconductor quantum rods in a cylindrical microcavity, *Adv. Mater.* **14**, 317, (2002).

7. SJ. Pearton, CR. Abernathy, DP. Norton, AF. Hebard, YD. Park, LA. Boatner and JD. Budai, Advances in wide bandgap materials for semiconductor spintronics. *Materials Science & Engineering*, **40**, 4 (2003).

8. S. A. Wolf, D. D. Awschalom, R. A. Buhrman, J. M. Daughton, S. von Molnar, M. L. Roukes, A. Y. Chtchelkanova, D. M. Treger, Spintronics: A spin-based electronics vision for the future, *Science*, **294**, 1490 (2001).

9. H. Ohno, Making nonmagnetic semiconductors ferromagnetic, *Science*, **281**, 951-956 (1998).

10. Y. Yamamoto, T. Miura, M. Suzuki, N. Kawamura, H. Miyagawa, T. Nakamura, K. Kobayashi, T. Teranishi, and H. Hori, Diameter dependence of ferromagnetic spin moment in Au nanocrystals, *Phys. Rev. B.* **69**. 174411 (2004).

11. Y. Yamamoto, T. Miura, M. Suzuki, N. Kawamura, H. Miyagawa, T. Nakamura, K. Kobayashi, T. Teranishi and H. Hori, Direct Observation of Ferromagnetic Spin Polarization in Gold Nanoparticles, *Phys. Rev. Lett.* **93**. 116801 (2004).

12. P. Crespo, R. Litran, M. Multigner, J.M. de la Fuente, J.C. Sanchez Lopez, M.A. Garcia, C. Lopez Cartes, A. Hernando, S. Penades, A. Fernandez, Permanent magnetism, magnetic anisotropy, and hysteresis of thiol-capped gold nanoparticles, *Phys. ReV. Lett.* **93**, 087204 (2004).

13. A. Hernando, P. Crespo, M.A. Garcı́a, E. Ferná́ndez Pinel, J.de la Venta, A. Ferná́ndez, S. Penade′s, Giant magnetic anisotropy at the nanoscale: Overcoming the superparamagnetic limit, *Phys. ReV. B,* **74**, 052403 (2006).

14. XW. Teng, M. Feygenson, Q. Wang, J. He, WX. Du, F. Anatoly, WQ Han, M. Aronson, Electronic and Magnetic Properties of Ultrathin Au/Pt Nanowires, *Nano. Lett,* **9**, 3177 (2009).

15. T. Mokari, E. Rothenberg, I. Popov, R. Costi and U. Banin, Selective Growth of Metal Tips onto Semiconductor Quantum Rods and Tetrapods, *Science.* **304**, 1787-1789 (2004).

16. T. Mokari1, C. G. Sztrum, A. Salant, E. Rabani and Uri Banin, Formation of asymmetric one-sidedmetal-tipped semiconductor nanocrystal dots and rods, *Nature Mater,* **4**, 855-863 (2005).

17. G. Menagen, J. E. Macdonald, Y. Shemesh, I. Popov and U. Banin, Au Growth on Semiconductor Nanorods: Photoinduced versus Thermal Growth Mechanisms, *J. Am. Chem. Soc.* **131**, 17406–17411 (2009).

18. Aaron E. Saunders, Inna Popov, and Uri Banin, Synthesis of Hybrid CdS-Au Colloidal Nanostructures, *J. Phys. Chem. B,* **110**, 25421-25429 (2006).

19. M. A. Garcia, J. M. Merino, E. Ferná́ndez Pinel, A. Quesada, J. de la Venta, M. L. Rú́z Gonzá́lez, G. R. Castro, P. Crespo, J. Llopis, J. M. Gonzá́lez-Calbet, and A. Hernando, Magnetic Properties of ZnO Nanoparticles, *Nano. Lett,* **7**, 1489 (2007).

20. F. Matsukura, H. Ohno, A. Shen, Y. Sugawara, Transport properties and origin of ferromagnetism in (Ga,Mn)As, *Phys. Rev. B,* **57**, R2037 (1998).

21. H. Ohno, A. Shen, F. Matsukura, A. Oiwa, A. Endo, S. Katsumoto, Y. Iye, (Ga,Mn)As: A new diluted magnetic semiconductor based on GaAs, *Appl. Phys. Lett.* **69**, 363 (1996).

22. B. Beschoten, P.A. Crowell, I. Malajovich, D.D. Awschalom, F. Matsukura, A. Shen, H. Ohno, Magnetic circular dichroism studies of carrier-induced ferromagnetism in (Ga1-xMnx)As *Phys. Rev. Lett.* 83, 3073 (1999).

23. M. Tanaka, Epitaxial growth and properties of III–V magnetic semiconductor (GaMn)As and its heterostructures, *J. Vac. Sci. Technol. B* **16**, 2267 (1998).

24. Y. Nagai, T. Kurimoto, K. Nagasaka, H. Nojiri, M. Motokawa, F. Matsukura, T. Dietl, H. Ohno, Spin polarization dependent far infrared absorption in Ga1-xMnxAs *Jpn. J. Appl. Phys.* **40**, 6231 (2001).

25. A. Shen, F. Matsukura, S.P. Guo, Y. Sugawara, H. Ohno, M. Tani, A. Abe, H.C. Liu, Low-temperature molecular beam epitaxial growth of GaAs and (Ga,Mn)As *J. Cryst. Growth,* **201**, 379 (1999).

26. D. Chiba, N. Akiba, F. Matsukura, Y. Ohno, H. Ohno, Magnetic properties of (Al,Ga,Mn)As, *Appl. Phys. Lett.* **77**, 1873 (2002).

27. H. Ohno, F. Matsukura, T. Owiya, N. Akiba, Spin-dependent tunneling and properties of ferromagnetic (Ga,Mn)As, *J. Appl. Phys.* **85**, 4277 (1999).

28. A. Oiwa, T. Slupinski, H. Munekata, Control of magnetization reversal process by light illumination in ferromagnetic semiconductor heterostructure p-(In, Mn)As/GaSb, *Appl. Phys. Lett.* **78,** 518 (2001).

29. S. Koshihara, A. Oiwa, M. Hirasawa, S. Katsumoto, Y. Iye, C. Urano, H. Takagi, H. Munekata, Ferromagnetic order induced by photogenerated carriers in magnetic III-V semiconductor heterostructures of (In,Mn)As/GaSb *Phys. Rev. Lett.* **78,** 4617 (1997).

CHAPTER 2 SYNTHESIS OF CdSe NANORODS

2.1 Introduction

The synthesis of II-VI and III-V semiconductors with precise controlling of various shapes has been intensively studied over the past decade. CdSe, as one of the II-VI semiconductors, becomes a popular choice for researchers due to its well-studied synthetic approaches and promising applications in biological labeling and light-emitting diodes [1]. CdSe nanostructures can be synthesized with various morphologies, such as spherical particle, rod, arrow, tear drop and tetrapod [2]. Among these shapes, CdSe nanorods have been proved as good substrates for Au nanoparticles to grow on [3-6]. Therefore, we selected CdSe nanorods as the host semiconductor to produce CdSe-Au hybrid nanorods in this work.

2.1.1 Shape Control of CdSe

CdSe nanocrystals can be made via the injection of reactant precursors into a hot excess surfactant solvent, such as mixture of trioctylphosphine oxide (TOPO, [$CH_3(CH_2)_7]_3PO$) and stearic acid ($CH_3(CH_2)_{16}COOH$) [1,2,7-9], which usually provides a fast nucleation of CdSe seeds, followed by slow growth. Two injecting methods are mostly adopted. One is a mono-injection method, from which the spherical CdSe nanoparticles are formed. In this method, the temporal separation between nucleation and growth helps to achieve relatively narrow size distribution of nanoparticles. The other is a multiple-injection method, from which CdSe nanorods are produced.

In the early study of CdSe synthetic methods, Murray *et al.* provided a simple route to the production of nearly monodispersed CdE (E = S, Se, Te) semiconductor nanoparticles [9]. A pre-heated (~300 °C) surfactant solvent was prepared first followed by co-injection of organometallic precursors (cadmium dimethyl, $Cd(CH_3)_2$ and Se trioctylphosphine, TOP, $[CH_3(CH_2)_7]_3P$) to produce a homogeneous nucleation using TOPO as a surfactant. The consequent growth at a moderate temperatures range (230~260 °C) resulted in the formation of uniform CdSe nanoparticles with diameters ranging from 1.5 to 11.5 nm.

Qu *et al.* developed a mono-injection method based on Murray's work to produce uniform CdSe nanoparticle system using [10]. In their method, $Cd(CH_3)_2$ was replaced by cadmium stearate ($Cd(C_{17}H_{35}COO)_2$ or $Cd(Ac)_2$), due to the concerns of flammability, high expense, and low stability even at room temperature in $Cd(CH_3)_2$. They adopted a mono-injection method to produce CdSe nanocrystals in the presence of stearic acid. Instead of co-injecting the mixture of Cd and Se precursors, a Se solution was injected in to a preheated mixture of $Cd(Ac)_2$ and surfactant (250-360 °C). By using $Cd(Ac)_2$ and this mono-injection method, Qu *et al.* achieved the production of CdSe nanoparticles ranging from 2 to 25 nm.

Peng *et al.* also developed Murray's method and first achieved the shape control of CdSe nanostructures from CdSe nanoparticles to CdSe nanorods using $Cd(CH_3)_2$ as precursor [1, 7]. However, instead of using pure TOPO, the mixture of hexylphosphonic acid (HPA, $CH_3(CH_2)_5P(O)(OH)_2$) and TOPO was used to serve as surfactant and reaction solvent. The function of HPA was to maintain the growth of CdSe nanorods in a controllable manner. Peng *et al.* also introduced multiple injections of organometallic

precursors in the synthesis, which replenished monomers during the growth period of CdSe and resulted in the anisotropic growth of CdSe nanorods. By adopting HPA as surfactant and using multiple-injection method, CdSe nanorods were successfully produced in their studies. It was indicated that the growth of hexagonal crystal structure (wurtzite) of CdSe was highly anisotropic. Some growth conditions favored crystallization along the <001> axis, usually called the c-axis of wurtzite structure, and resulted in the formation of the CdSe nanorods. However, the initial injection temperature adopted in this method was in the range from 340 °C to 360 °C. Also, this multiple-injection method is relatively complex to execute compared to the mono-injection method adopted in the synthesis of CdSe nanoparticles.

Shieh *et al.* further explored Peng's multiple-injection approach in the synthesis of CdSe nanorods using cadmium mono-oxide (CdO) as precursor, and n-tetradecylphosphonic acid (TDPA, $CH_3(CH_2)_{13}P(O)(OH)_2$) and TOPO as surfactant [8]. They adopted a lower injection temperature (260 °C). However, they had to preheat the Se precursors to 120 °C every time before the injection.

From above discussion we can extract three important factors in the synthesis of CdSe nanocrystals: (1) In the synthesis of CdSe nanoparticles, $Cd(Ac)_2$ can be used as a precursor, avoiding high risk $Cd(CH_3)_2$ [10]; (2) a simple mono-injection method could be carried out using HPA as surfactant, avoiding the traditional co-injection method [10]; (3) in the synthesis of nanorods, multiple-injection method is commonly used to synthesize nanorods [1, 2, 7-9].

In this work, we developed a mono-injection method based on traditional approach used in the synthesis of CdSe nanocrystals. We successfully achieved the shape control of CdSe nanostructures from nanoparticles to nanorods by simply adjusting the molar ratios between Se and Cd precursors. The growth models were proposed for different morphologies of CdSe and verified by the followed experimental results. The synthesized CdSe nanorods are utilized for the growth of Au nanoparticles which will be interpreted in details in the next chapter.

2.2 Synthesis of CdSe

In this work, we used $Cd(Ac)_2$ as the Cd precursor, a mixture of TOPO, octadecylamine (ODA, $CH_3(CH_2)_{17}NH_2$) and stearic acid as reaction solvent and surfactants. Se powder was dissolved in TOP to serve as injection solution for the growth of CdSe nanocrystals. The injection temperature was 310 °C and the growth time period for CdSe nanocrystals was 25 min. In a typical synthesis of CdSe, a mixture of $Cd(Ac)_2$ (90%, Strem Chemicals, 0.1132 g or 0.15 mmol), stearic acid (98%, Alfa Aesar, 0.0853 g or 0.3 mmol), TOPO (98%, Alfa Aesar, 2.5 g or 6.3 mmol) and ODA (90%, Acros, 2.5 g or 8.3 mmol) were added into a 50 ml three-neck round-bottom flask and then heated up via a heating mantle under vigorous stirring and argon flow protection. During the heating process, the initial white solid mixture turned into a transparent colorless solution. When the solution temperature reached 310 °C, a Se solution made by dissolving 0.18, 0.25, 0.75 or 1.0 mmol Se powder (99%, Strem Chemicals) into 1.79, 2.02, 5.38 or 7.17 mmol TOP (90%, Alfa Aesar) was quickly injected into the flask (<< 1 s). A dark purple solution formed immediately. After heating for an additional 25 min, the reaction was stopped by the removal of the heating mantle. After the solution was cooled to around

60 °C, the reaction solution was equally distributed into two 14 ml plastic centrifugation tubes. The final precipitation of CdSe was collected by washing it with ethanol and chloroform via a high speed centrifugation process. The flow chart of the synthesis of CdSe is shown in **Figure 2.1**.
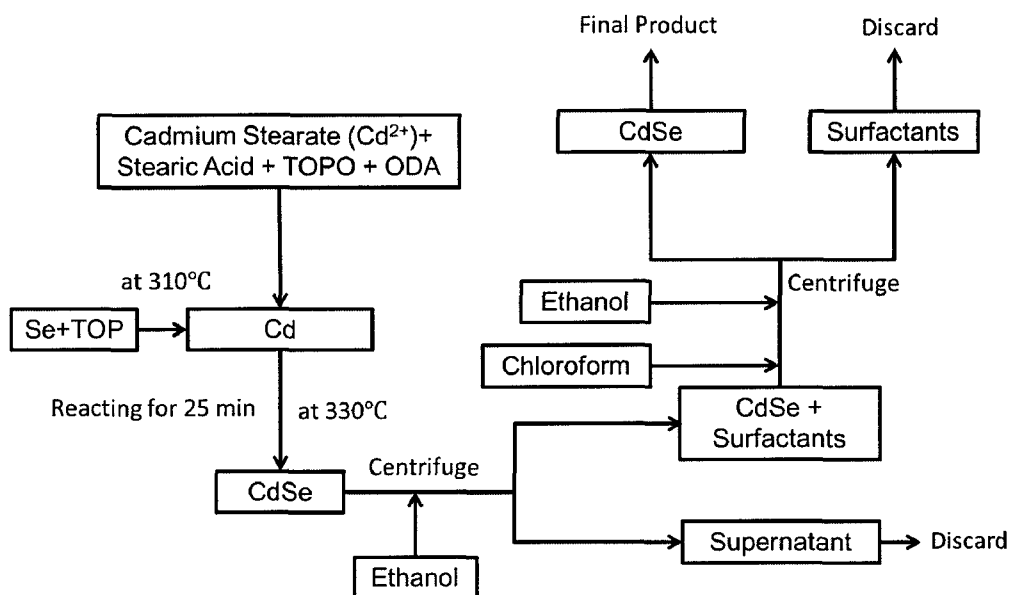
Figure 2.1 Flow chart of the synthesis of CdSe

2.3 Material Characterizations

2.3.1 Transmission Electron Microscope

A Zeiss/LEO 922 Omega transmission electron microscope (TEM) with accelerating voltages of 120 kV was used to observe the morphologies of CdSe nanostructures. The TEM sample was prepared by dropping 0.02~0.04 mg of CdSe nanocrystals in chloroform solution on a carbon-coated copper grid. The sample was dried at room temperature.

2.3.2 Energy Dispersive Spectroscopy

An AMR 3300FE scanning electron microscopy (SEM) equipped with a PGT Imix-PC energy-dispersive X-ray (EDS) microanalysis system was used to analyze the chemical compositions of CdSe nanocrystals. The EDS sample was prepared by dropping 1.0~1.2 mg of CdSe nanocrystals chloroform solution onto the carbon tape. The sample was dried under room temperature before measurement.

2.4 Result and Discussion

2.4.1 Effect of Se/Cd Molar Ratios on the Morphologies of CdSe

A series of syntheses using a Se/Cd molar ratio of 5 was first conducted. Though the synthetic conditions were kept the same through all the syntheses, CdSe nanocrystals with different morphologies were produced. The morphologies of these CdSe nanocrystal systems can be classified into three categories: (A) CdSe nanoparticles, (B) CdSe nanorods, and (C) mixtures of CdSe nanoparticles and CdSe nanorods. **Figure 2.2** to **2.4** shows the TEM images of these three different CdSe nanostructures, all of which were synthesized using a Se/Cd molar ratio of 5 at 310 °C (injection temperature) and reacting for 25 min.

In the first batch, a homogenous CdSe nanoparticles system was produced. The average diameter of the CdSe nanoparticles was 4.7 ± 0.7 nm as shown in **Figure 2.2**.
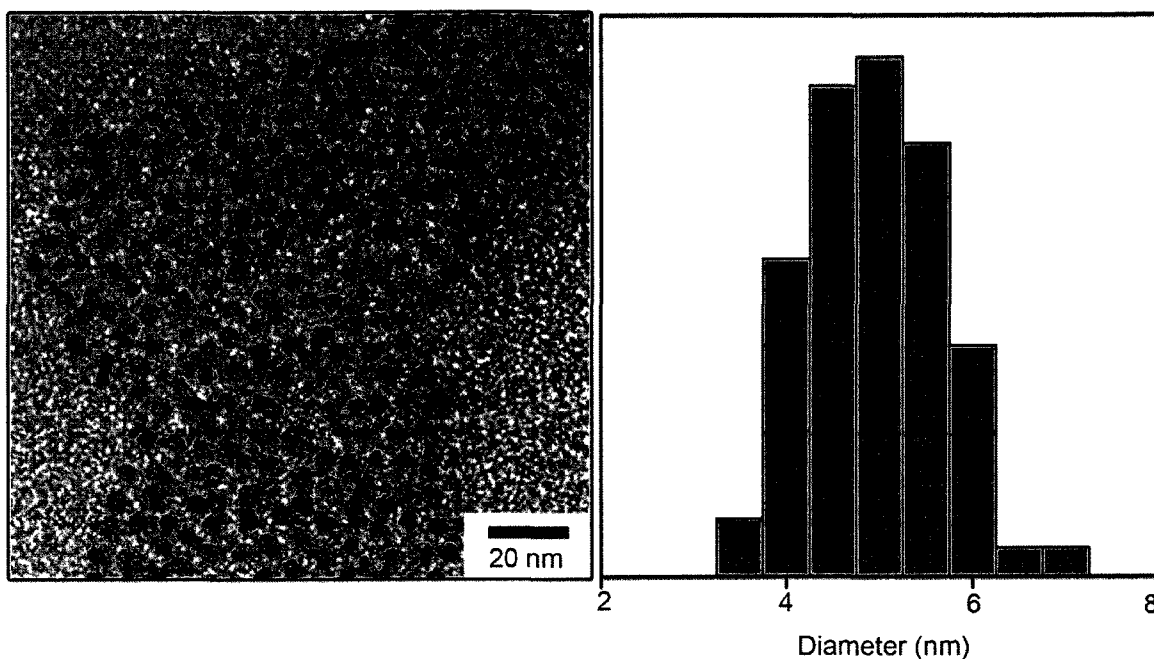
Figure 2.2 TEM images of CdSe nanoparticles and the corresponding sizing histogram. These CdSe nanoparticles were synthesized at 310 °C for 25 min using Cd(Ac)$_2$ (0.15 mmol), CH$_3$(CH$_2$)$_{16}$COOH (0.3 mmol), TOPO (2.5 g), ODA (2.5 g), Se (0.75 mmol) and TOP (5.38 mmol). The molar ratio of Se/Cd was 5. The average diameter of CdSe nanoparticles was 4.7 ± 0.7 nm.

In the second batch, a homogenous CdSe nanorod system was produced. The average length of the rods was 33.4 ± 20.4 nm, while the average width was 7.1 ± 1.2 nm as shown in **Figure 2.3**.
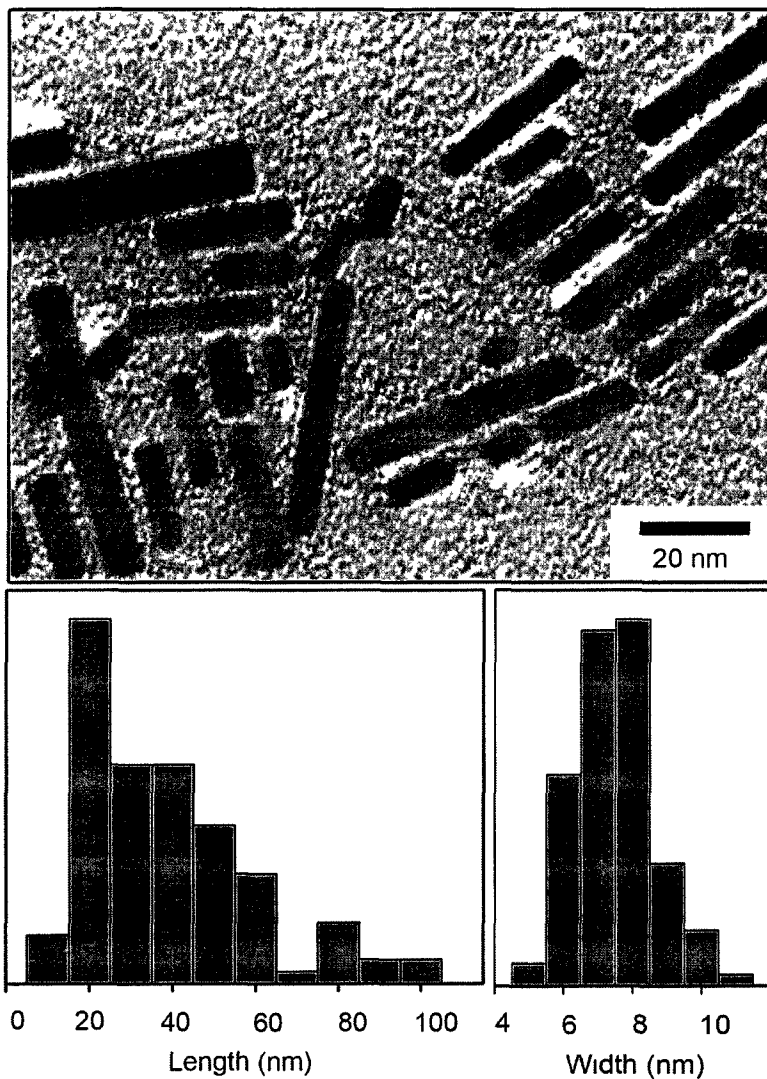
Figure 2.3 TEM images of CdSe nanorods and the corresponding sizing histograms. These CdSe nanorods were synthesized at 310 °C for 25 min using $Cd(Ac)_2$ (0.15 mmol), $CH_3(CH_2)_{16}COOH$ (0.3 mmol), TOPO (2.5 g), ODA (2.5 g), Se (0.75 mmol) and TOP (5.38 mmol). The molar ratio of Se/Cd was 5. The length of the rod was 33.4 ± 20.4 nm, the width was 7.1 ± 1.2 nm.
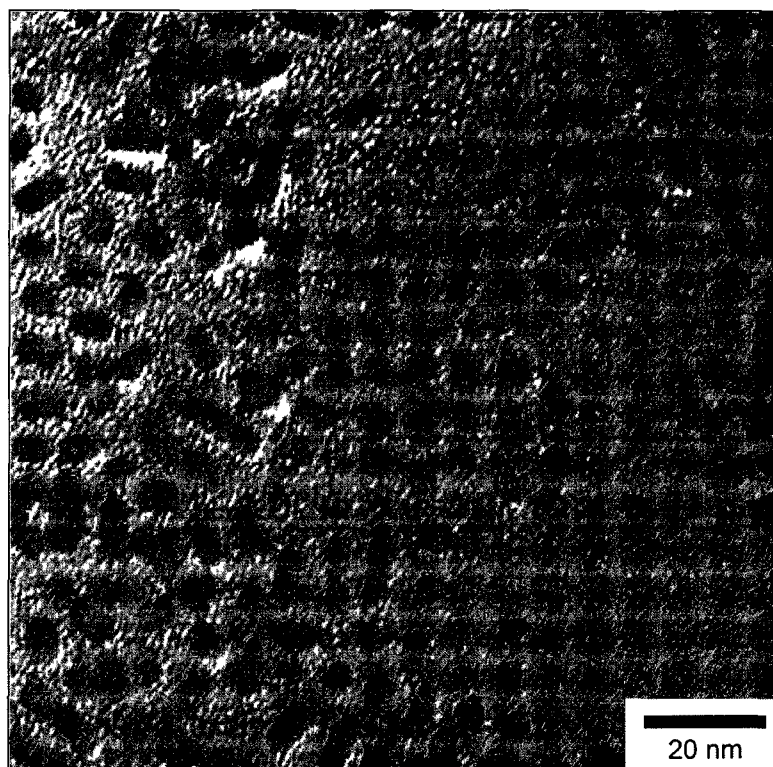
Figure 2.4 TEM images of mixture of CdSe nanoparticles and nanorods. In this system about 40% of CdSe nanocrystals were nanorods, and 60% were nanoparticles. These CdSe nanocrystals were synthesized at 310 °C for 25 min using $Cd(Ac)_2$ (0.15 mmol), $CH_3(CH_2)_{16}COOH$ (0.3 mmol), TOPO (2.5 g), ODA (2.5 g), Se (0.75 mmol) and TOP (5.38 mmol). The molar ratio of Se/Cd was 5. The average diameter of nanoparticles was 5.2 ± 0.8 nm. The length of the rod was 13.6 ± 3.8 nm, while the width was 3.8 ± 0.4 nm.

The contradicted experimental results indicated that under the Se/Cd molar ratio of 5, it was hard to synthesize reproducible CdSe nanocrystals. Moreover, the observation of both CdSe nanoparticles and nanorods indicate that 5 might be a critical molar ratio between Se and Cd to form different shaped CdSe nanocrystals. To get reproducible CdSe nanorods, it was necessary to study the growth model of CdSe.

2.4.2 Growth Models for CdSe with Different Morphologies

During the synthesis of CdSe, $Cd(Ac)_2$ first decomposed to form Cd atoms at high temperatures [2]. These Cd atoms or clusters (aggregation of a few atoms) didn't nucleate

before reaching the supersaturation. The formation of CdSe nanocrystals was triggered by injecting the Se/TOP solution into the flask. After injection, the Cd monomers reacted with Se to form CdSe monomers immediately, judging by the fast color changes upon the injection of Se into reaction solution. Once the concentration of CdSe reached supersaturation level, the CdSe nuclei (seeds) formed in the solution. In the meantime, CdSe monomers continued to deposit on CdSe nuclei, and resulted in the further growth of CdSe nanostructures. The continuous growth of CdSe nanostructures depleted the CdSe monomers in the solution, which would eventually decrease to the equilibrium concentration (the lowest concentration of CdSe monomer in solution).

In the synthesis of CdSe with the molar ratio of Se/Cd=5, both nanorods and nanoparticles were observed. It is known that the formation of CdSe nanorods could be attributed to the elongation of c-axis in CdSe crystal structure [2]. Namely, if the c-axis has a faster growth rate comparing to other axes in CdSe crystal structure, CdSe nanorods will be formed via an anisotropic growth along c-axis; if all the axes have a similar growth rate, CdSe nanoparticles will form via an isotropic growth. The growth rates of different axes can be also affected by the concentration of monomers in the solution. If the concentration of monomers is very high, all the axes will have a similar growth rate, CdSe nanoparticles will be formed; if the concentration of the monomers is low, CdSe nanorods will be formed via a dominant growth along c-axis. The corresponding scheme for the isotropic and anisotropic growth of CdSe nanocrystals is shown in **Figure 2.5**.
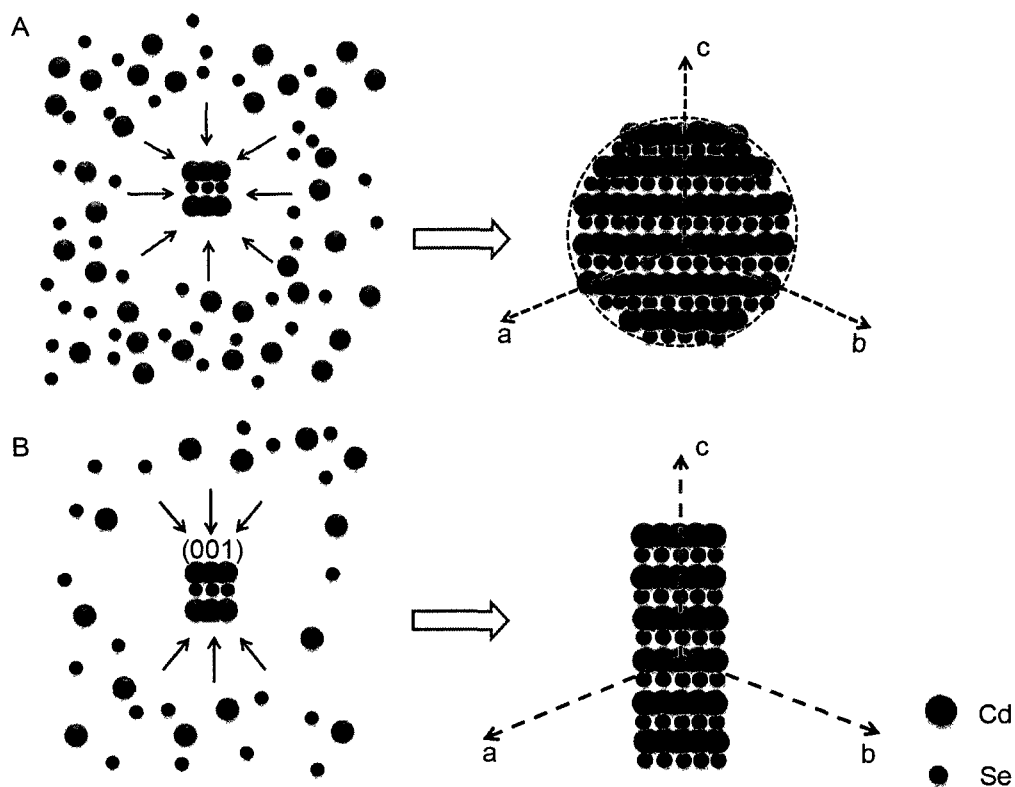
Figure 2.5 (**A**) Isotropic growth of CdSe nanoparticles. (**B**) Anisotropic growth of CdSe nanorods. (001) is the crystal surface perpendicular to the c-axis in the CdSe structure.

In order to verify the effect of CdSe concentration on the morphologies of CdSe as proposed in **Figure 2.5**, a series of experiments was conducted using different Se/Cd molar ratios. To simplify the experimental procedure, we kept the amount of $Cd(Ac)_2$ constant, and only adjusted the amount of Se to change the molar ratios of Se/Cd in the syntheses. If the model we proposed is valid, high amount of Se will lead to the formation of CdSe nanoparticles via the isotropic growth; while fewer amount of Se will lead to the formation of CdSe nanorods by encouraging the growth along c-axis. The amounts of Cd and Se used in the syntheses are in **Table 2.1,** and the TEM images of resulting CdSe nanostructures are shown in **Figure 2.6, 2.7** and **2.8.**

Table 2.1 Molar Ratios of Se/Cd Adopted in the Syntheses of CdSe

Condition	1	2	3	4
Cd(Ac)$_2$/mmol	0.15	0.15	0.15	0.15
Se/mmol	0.18	0.25	0.75	1.0
TOP/mmol	1.79	2.02	5.38	7.17
Molar Ratios of Se/Cd	1.2	1.7	5	6.7

When Se/Cd molar ratio was equal to 6.7, CdSe crystals grow isotropically during the reaction due to the abundant existence of monomers in the solution (**Figure 2.6**).
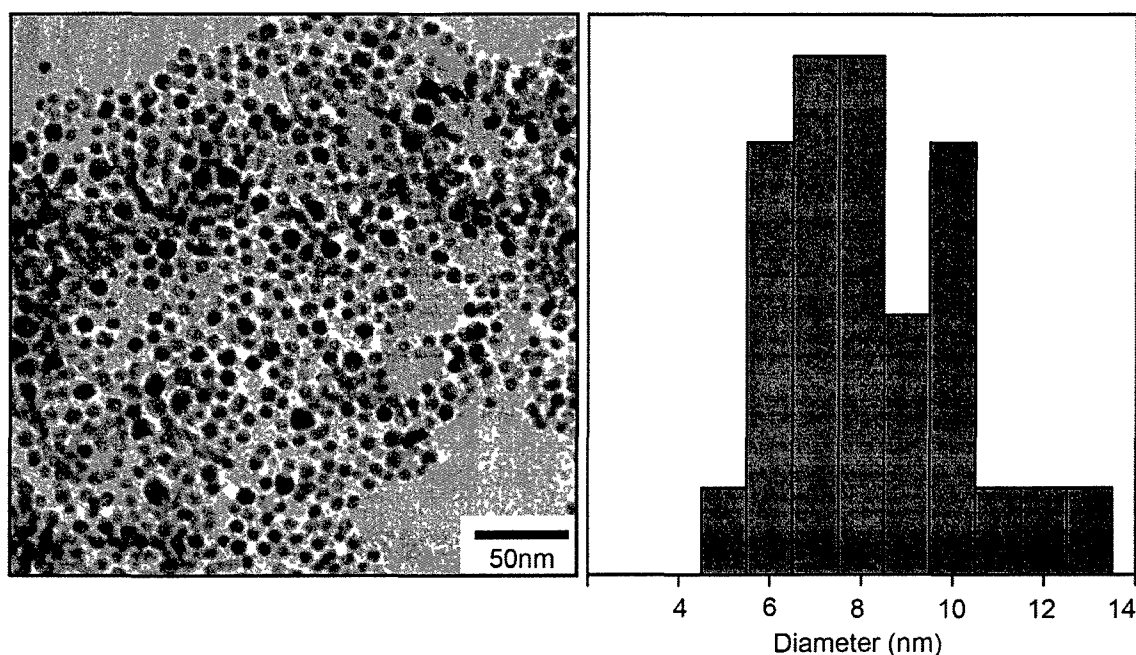
Figure 2.6 TEM images of CdSe nanoparticles and the corresponding sizing histogram. These CdSe nanoparticles were synthesized at 310 ℃ for 25 min using Cd(Ac)$_2$ (0.15 mmol), CH$_3$(CH$_2$)$_{16}$COOH (0.3 mmol), TOPO (2.5 g), ODA (2.5 g), Se (1 mmol) and TOP (7.17 mmol). The molar ratio of Se/Cd was 6.7. The average diameter of CdSe nanoparticles was 7.7 ± 1.9 nm.

When the Se/Cd molar ratios decreased to 1.7 and 1.2 in the syntheses, the CdSe nanorod systems were synthesized (**Figure 2.7** and **2.8**). The observations are well consistent with the growth models we proposed. Moreover, compared to previous

reported methods [1-7], the experimental procedure presenting in this work is more easily to conduct. This method allows the synthesis to conduct at a moderate temperature. Also by simply changing the molar ratios between Se and Cd, different shaped CdSe nanocrystals can be successfully synthesized, which provides a new thought to control the shape of CdSe nanocrystals.
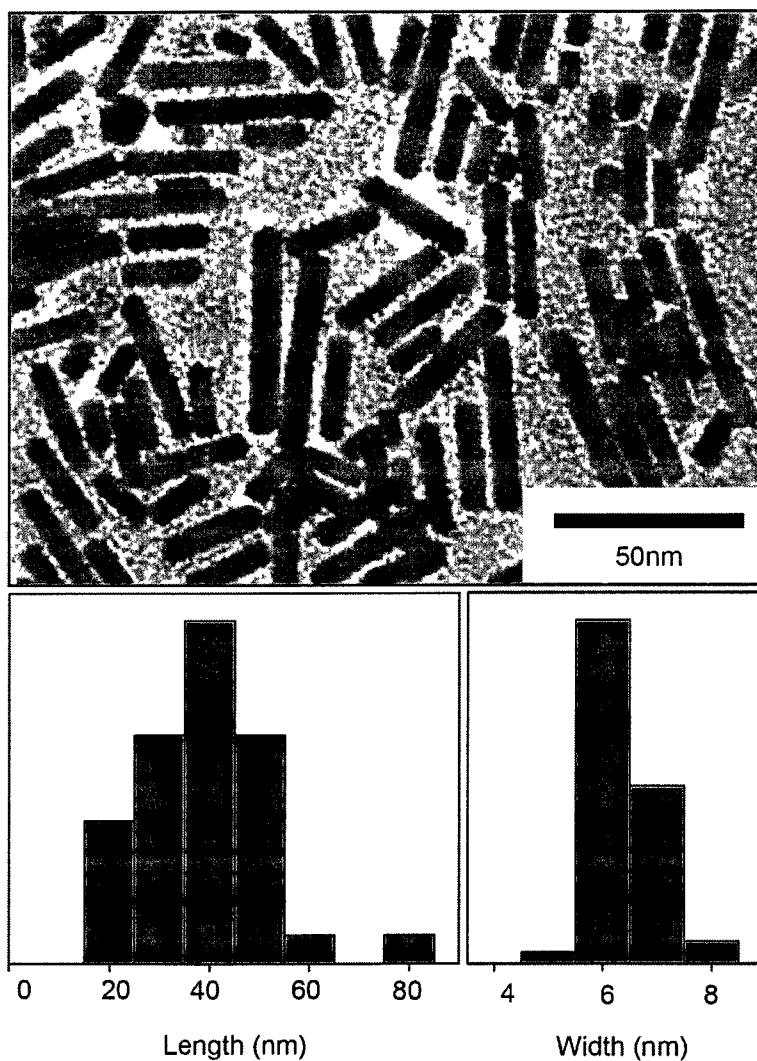
Figure 2.7 TEM images of CdSe nanorods and the corresponding sizing histograms. These CdSe nanorods were synthesized at 310 °C for 25 min using $Cd(Ac)_2$ (0.15 mmol), $CH_3(CH_2)_{16}COOH$ (0.3 mmol), TOPO (2.5 g), ODA (2.5 g), Se (0.25 mmol) and TOP (2.02 mmol). The molar ratio of Se/Cd was 1.7. The length of the rod was 33.4 ± 13.0 nm, the width was 5.9 ± 0.5 nm.
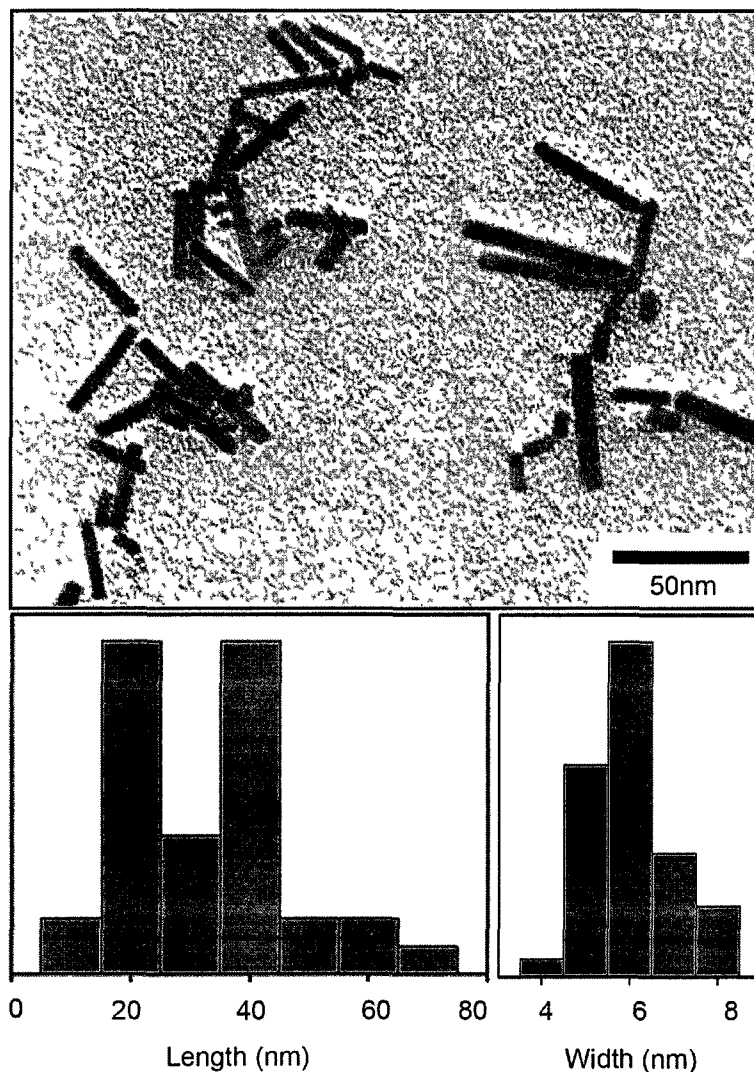
Figure 2.8 TEM images of CdSe nanorods and the corresponding sizing histograms. These CdSe nanorods were synthesized at 310 °C for 25 min using $Cd(Ac)_2$ (0.15 mmol), $CH_3(CH_2)_{16}COOH$ (0.3 mmol), TOPO (2.5 g), ODA (2.5 g), Se (0.15 mmol) and TOP (1.79 mmol). The molar ratio of Se/Cd was 1.2. The length of the rod was 27.0 ± 14.4 nm, the width was 5.6 ± 0.9 nm.

2.5 Conclusions

In summary, a simple mono-injection method was adopted in the synthesis of CdSe nanocrystals. CdSe nanoparticles and nanorods were produced by adjusting the molar ratios between Se and Cd precursors. We proposed a plausible growth model in which the

concentration of monomers in the solution played an important role in determining the final morphologies of CdSe nanocrystals. The model can be briefly described as high concentrations of CdSe monomer lead to an isotropic growth of CdSe nanoparticles; while low concentrations of CdSe monomer lead to an anisotropic growth of CdSe nanorods. A series of experiments using different Se/Cd molar ratios (Se/Cd = 6.7, 1.7 and 1.2) was carried out to verify this growth model.

References:

1. XG. Peng, L. Manna, W. Yang, J. Wickham, E. Escher, A. Kadavanich, A. P. Alivisatos, Shape control of CdSe nanocrystals, *Nature,* **404**, 59-61 (2000).

2. L. Manna, E. C. Scher, Synthesis of soluble and processable rod-, arrow-, teardrop-, and tetrapod-shaped CdSe nanocrystals, A. P. Alivisatos, *J. Am. Chem. Soc.* **122**, 12700-12706 (2000).

3. T. Mokari, E. Rothenberg, I. Popov, R. Costi and U. Banin, Selective Growth of Metal Tips onto Semiconductor Quantum Rods and Tetrapods, *Science.* **304**, 1787-1789 (2004).

4. T. Mokari1, C. G. Sztrum, A. Salant, E. Rabani and Uri Banin, Formation of asymmetric one-sidedmetal-tipped semiconductor nanocrystal dots and rods, *Nature Mater,* **4**, 855-863 (2005).

5. G. Menagen, J. E. Macdonald, Y. Shemesh, I. Popov and U. Banin, Au Growth on Semiconductor Nanorods: Photoinduced versus Thermal Growth Mechanisms, *J. Am. Chem. Soc.* **131**, 17406–17411 (2009).

6. Aaron E. Saunders, Inna Popov, and Uri Banin, Synthesis of Hybrid CdS-Au Colloidal Nanostructures, *J. Phys. Chem. B*, **110**, 25421-25429 (2006).

7. Z. A. Peng and XG. Peng, Mechanisms of the shape evolution of CdSe nanocrystals, *J. Am. Chem. Soc.* **123**, 1389-1395 (2001).

8. F. Shieh, A. E. Saunders, B. A. Korgel, General shape control of colloidal CdS, CdSe, CdTe quantum rods and quantum rod heterostructures, *Phys. Rev. B. Lett*, **109**, 8538-8542 (2005).

9. C. B. Murray, D. J. Norris, and M. G. Bawendi, Synthesis and characterization of nearly monodispersed CdE (E = S, Se, Te) semiconductor Nano crystallites, *J. Am. Chem. Soc.* **115**, 8706-8715 (1993).

10. LH. Qu, Z. A. Peng, and XG. Peng, Alternative routes toward high quality CdSe nanocrystals, *Nano Lett*, **1**, 333-337 (2001).

11. XG. Peng, J. Wickham, and A. P. Alivisatos, Kinetics of II-VI and III-V colloidal semiconductor nanocrystal growth: "Focusing" of size distributions, *J. Am. Chem. Soc.* **120**, 5343-5344 (1998).

CHAPTER 3 SYNTHESIS OF CdSe-Au NANORODS

3.1 Introduction

Due to their unique room-temperature ferromagnetism, Au nanoparticles may become magnetic dopants for DMS applications. In order to realize the ferromagnetism of Au nanoparticles, Au nanoparticles with sizes less than 3 nm are highly demanded in this study [1-4].

The growth of metals on semiconductors as a means of increasing functionalities is an important subject in material science. A preparation of such hybrids usually involves the injection of a metal salt into the semiconductor nanocrystal solution. Mokari *et al.* first achieved a position-selective growth of Au nanoparticles onto CdSe nanorods by gradually adding gold chloride ($AuCl_3$) solution into CdSe nanorods solution at room temperature in the presence of dodecyldimethylammonium bromide (DDAB, $[CH_3(CH_2)_{11}]_2N(CH_3)_2Br,$) and dodecylamine ($CH_3(CH_2)_{11}NH_2$) [5]. They claimed that amine reduced $AuCl_3$ to form CdSe/Au hybrid with Au nanoparticles deposited on the tips of CdSe nanorods. Furthermore, by controlling the reaction times, the sizes of Au nanoparticles could be tuned from 2 to 4 nm. The most compelling aspect of Mokari's work was the high selective growth onto the rod's tips. They attributed this position-selective growth to higher surface energies of the tips, and more accessible sites due to imperfect passivation of surfactants on the tips of CdSe nanorods. In their follow-up work, Mokari *et al.* further studied the growth process of Au nanoparticles on CdSe nanorods [6-8]. At long reaction times, the concentration of $AuCl_3$ in solution dropped to a critical

value and the reaction transitioned from a growth state to a ripening state, resulting in the disappearance of small Au nanoparticles along the surface of nanorod and the growth of large Au nanoparticles on the tips of nanorod.

From the above discussion we can conclude two important factors to achieve the growth of Au nanoparticles on CdSe nanorods: (1) the growth of Au nanoparticles onto CdSe nanorods can be realized via a room-temperature reaction in the presence of DDAB and dodecylamine [5, 6]; (2) longer reaction time yields larger Au nanoparticles due to the ripening process [7, 8]. Since in the ideal Au-based DMS, the growth of small Au nanoparticles has to achieve a uniform distribution all over the surfaces of CdSe nanorods, not only on some particular sites on CdSe nanorods, an alternative method to achieve the uniform growth of Au nanoparticles all over the surfaces of CdSe nanorods is required.

3.2 Experimental Method

The Au precursor stock solution was prepared by dissolving 12 mg (0.04 mmol) of $AuCl_3$ (99.99%, Alfa Aesar), 15 mg (0.05 mmol) of 1-dodecyltrimethylammonium bromide (DTAB, $C_{12}H_{25}(CH_3)_3NBr$, 99%, Alfa Aesar) in 2 ml of chloroform at room temperature. The color of the $AuCl_3$ solution changed to yellow from orange after 5 min sonication. 0.15 mmol of as-synthesized CdSe nanorods with 30 mg TOPO ($C_{24}H_{51}OP$, 98%, Alfa Aesar) and 30 mg Octadecylamine (ODA, $CH_3(CH_2)_{17}NH_2$, 90%, Acros) were dissolved in 12 ml of chloroform in a 50 ml three-neck round-bottom flask under vigorous stirring and argon protection. Au precursor stock solution (0.167 ml) containing 1 mg (0.003 mmol) of $AuCl_3$ was injected into the reaction flask within 10 seconds. The reaction was carried out under room temperature. The TEM samples of CdSe-Au hybrid

nanorods were prepared by taking 0.3 ml reaction solution from the flask at several time intervals after the initial injection. After 5, 7, 10, 30 or 60 min, the samples were collected into a 14 ml centrifuge tube and centrifuged for 5 min to get the final products.

3.3 Galvanic Replacement Reaction between AuCl₃ and CdSe Nanorods

The galvanic replacement reaction usually involves a redox process. The driving force of this process is the reduction potential (E^{Θ}) difference between two reactants, with one reactant acting as the oxidizer and the other reactant as the reducer. Since E^{Θ} (Au^{3+}/Au^{0}) has higher reduction potential than E^{Θ} (Se^{2-}/Se^{4+}) (**Table 3.1**), the following reaction would happen in the solution:

$$2AuCl_3 + CdSe \rightarrow 2Au + Cd^{2+} + Se^{4+} + 6Cl^{-}$$
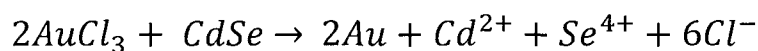
Table 3.1 Standard Reduction Potentials of Metal Ions in the Solution*

Reagents	E^{Θ} (Au^{3+}/Au)	E^{Θ} (Cd^{2+}/Cd)	E^{Θ} (Se^{2-}/Se)	E^{Θ} (Se/Se^{4+})	E^{Θ} (Se^{2-}/Se^{4+})
E^{Θ} / V	1.52	-0.40	0.11	-0.74	-0.64

*The values are measured under 25 °C, 1 atm in acidic solution[13].

After mixing with CdSe, Au^{3+} ions were reduced by Se^{2-} to form Au atoms at the surfaces of CdSe nanorods. As reaction went on, Au nuclei formed on the surfaces of CdSe nanorods, as shown in **Figure 3.1**.
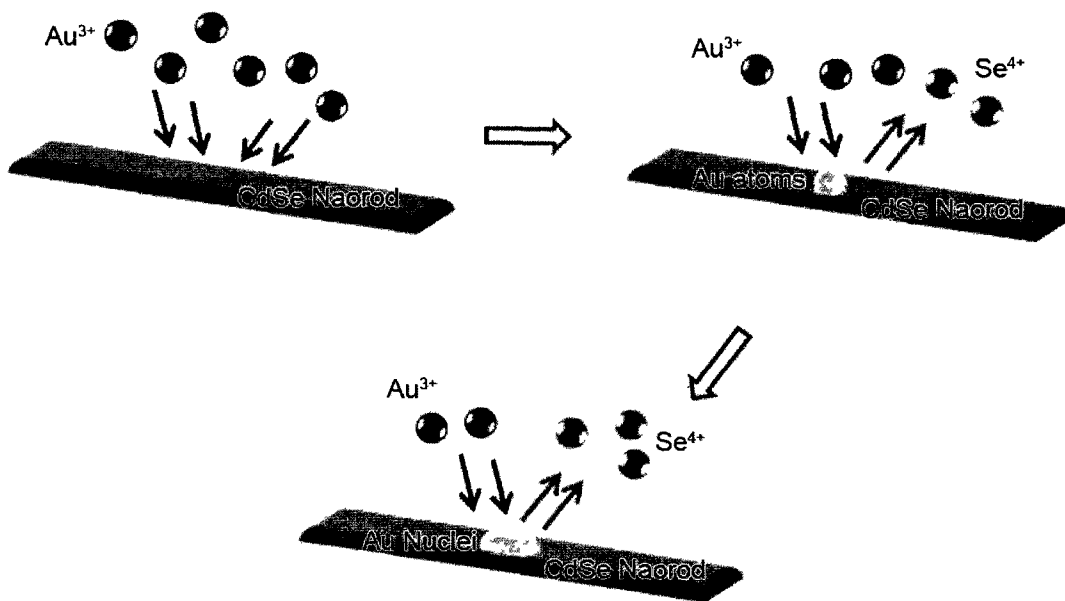
Figure 3.1 The galvanic replacement reactions between CdSe and AuCl₃ and the formation of the Au nuclei.

3.4 Results and Discussion

3.4.1 The Effect of AuCl₃ Amounts on the Sizes of Au Nanoparticles

In order to find the optimal concentration of $AuCl_3$ on the formation of Au nanoparticles, two different amounts of $AuCl_3$ were adopted in the reactions. **Figure 3.2** and **3.3** show TEM images of CdSe-Au hybrid nanorods synthesized using 0.015 mmol and 0.003 mmol $AuCl_3$ respectively. When the amount of $AuCl_3$ was 0.015 mmol, the size of Au nanoparticles was 6.0 ± 2.0 nm. When the amount of $AuCl_3$ was 0.003 mmol, the size of Au nanoparticles was 1.7 ± 0.5 nm. According to the literatures, the ferromagnetism of Au nanoparticles could be observed when the sizes of Au nanoparticles were less than 3 nm [1-4]. Thus, in order to produce ferromagnetic Au nanoparticles, 0.003 mmol of $AuCl_3$ was adopted in the follow-up experiments.
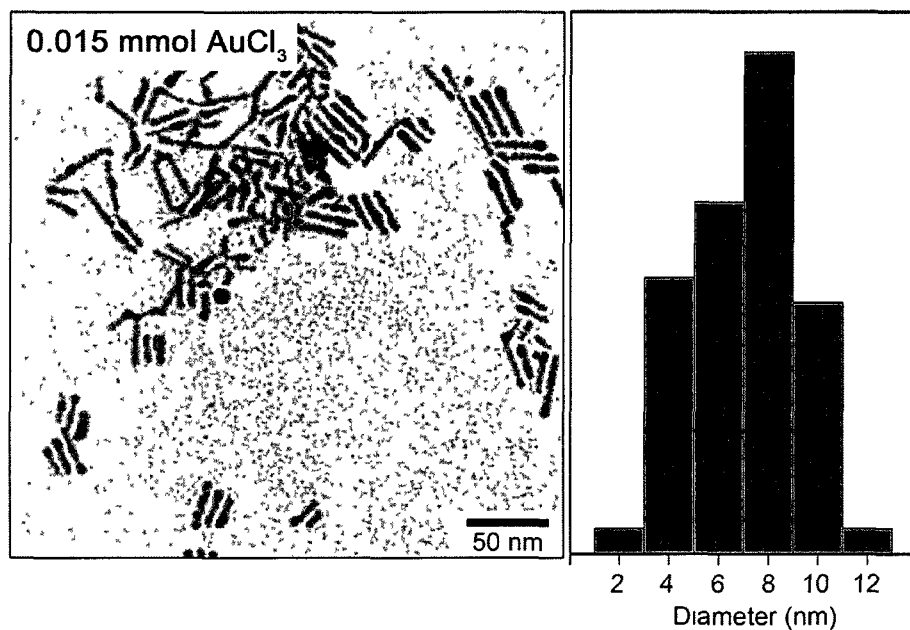
Figure 3.2 TEM image of CdSe-Au nanorods after 5 min reactions and the corresponding sizing histograms. These hybrid nanorods were synthesized by injecting 0.015 mmol $AuCl_3$ into 0.15 mmol as-synthesized CdSe nanorods solution. The average diameter of Au nanoparticles was 6.0 ± 2.0 nm.

Figure 3.3 TEM image of CdSe-Au nanorods after 5 min reactions and the corresponding sizing histograms. These hybrid nanorods were synthesized by injecting 0.003 mmol $AuCl_3$ into 0.15 mmol as-synthesized CdSe nanorods solution. The average diameter of Au nanoparticles was 1.7 ± 0.5 nm.

3.4.2 The Effect of the Reaction Time on the Sizes of Au Nanoparticles

In the syntheses of CdSe-Au hybrid nanorods, the reaction times varied from 5 to 60 min to control the sizes of Au nanoparticles. The CdSe nanorods used for reaction were synthesized using a Se/Cd molar ratio of 1.7. The molar numbers of CdSe nanorods and $AuCl_3$ was 0.15 mmol and 0.003 mmol.

Figure 3.4 to **3.9** shows TEM images of original CdSe nanorods and CdSe-Au hybrid nanorods synthesized at 5, 7, 10, 30 and 60 min. The average sizes of Au nanoparticles which were summarized in **Table 3.2**.

Table 3.2 Average Sizes of Au Nanoparticles at Different Reaction Times.

Reaction Time (min)	5	7	10	30	60
Size of Au (nm)	1.7 ± 0.6	1.9 ± 0.8	2.3 ± 0.7	2.3 ± 1.3	2.4 ± 0.9
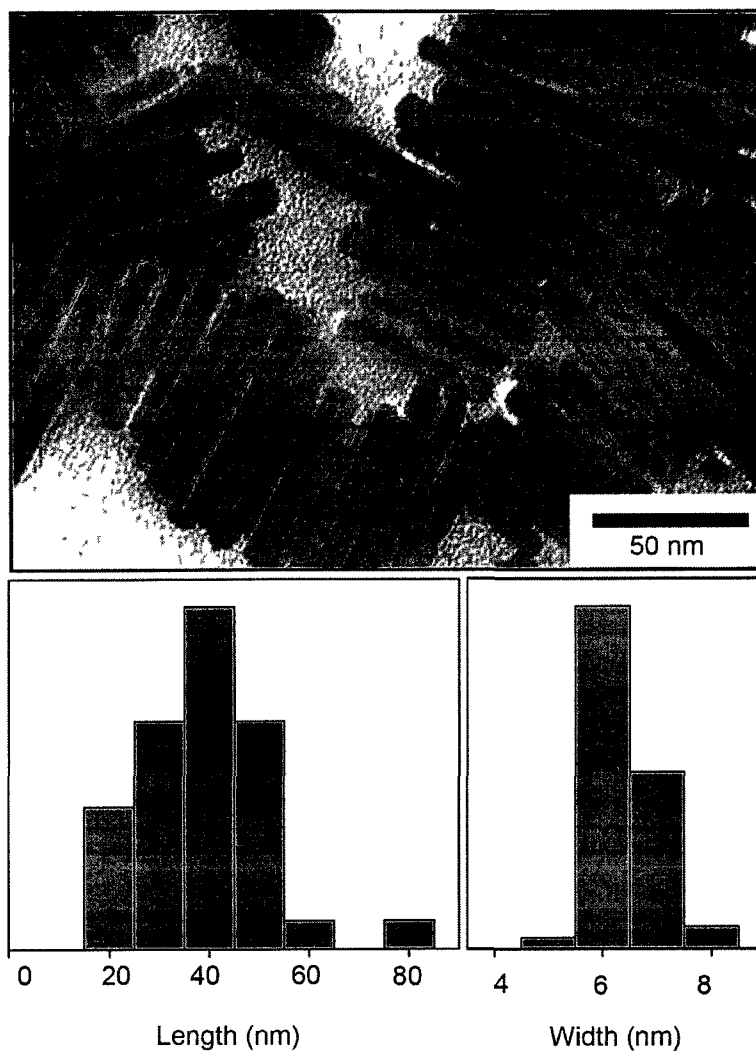
Figure 3.4 TEM image of CdSe nanorods and the corresponding sizing histograms. These CdSe nanorods were synthesized at 310 ℃ for 25 min using $Cd(Ac)_2$ (0.15 mmol), $CH_3(CH_2)_{16}COOH$ (0.3 mmol), TOPO (2.5 g), ODA (2.5 g), Se (0.25 mmol) and TOP (2.02 mmol). The molar ratio of Se/Cd was 1.7. The average length of the rods was 33.4 ± 20.4 nm; the average width was 5.9 ± 0.5 nm.

Figure 3.5 Original and enlarged TEM images of CdSe-Au hybrid nanorods and Au sizing histogram after 5 min reactions. These hybrid nanorods were synthesized by injecting 0.003 mmol $AuCl_3$ into 0.15 mmol as-synthesized CdSe nanorods solution. The average diameter of Au nanoparticles was 1.7 ± 0.5 nm.

Figure 3.6 Original and enlarged TEM images of CdSe-Au hybrid nanorods and Au sizing histogram after 7 min reactions. These hybrid nanorods were synthesized by injecting 0.003 mmol $AuCl_3$ into 0.15 mmol as-synthesized CdSe nanorods solution. The average diameter of Au nanoparticles was 1.9 ± 0.8 nm.
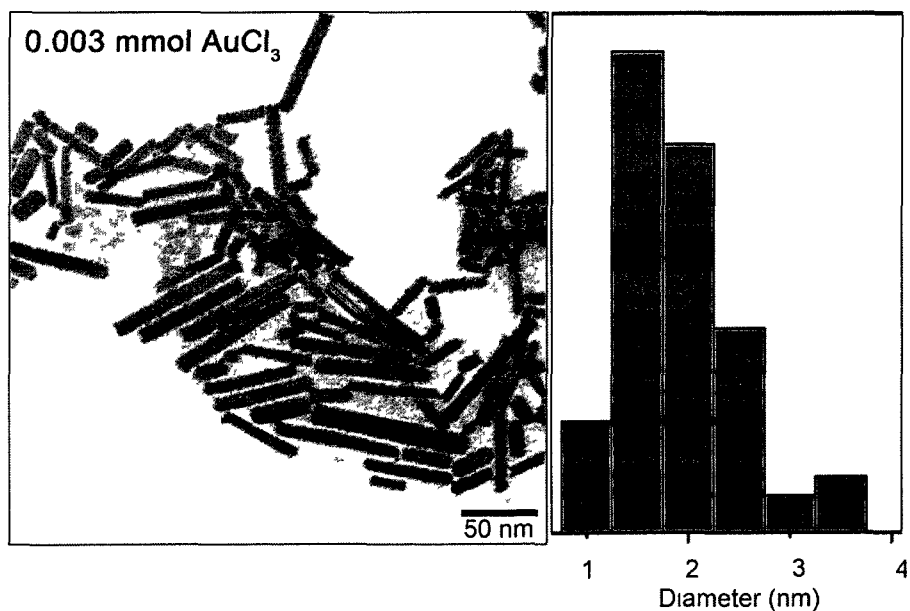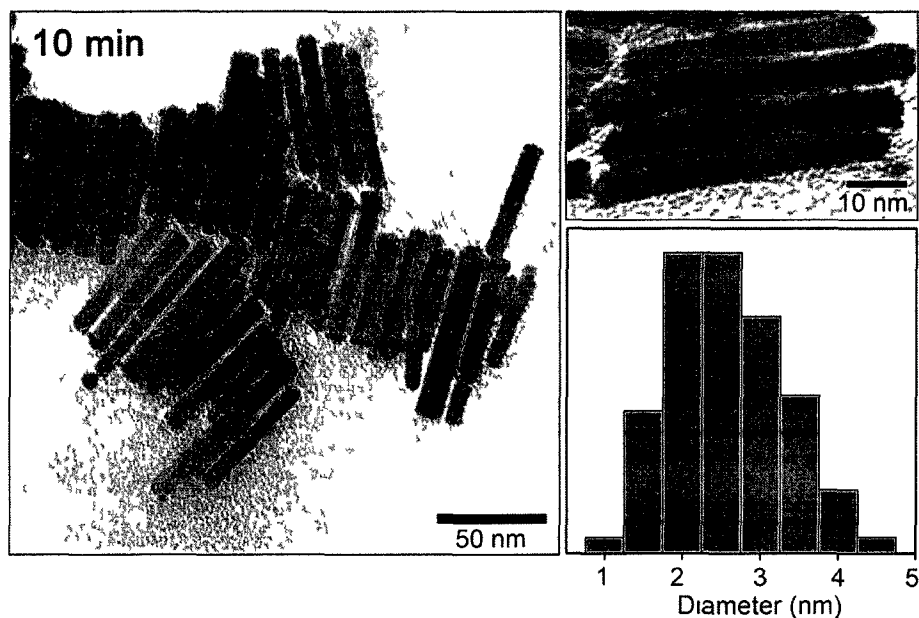
Figure 3.7 Original and enlarged TEM images of CdSe-Au hybrid nanorods and Au sizing histogram after 10 min reactions. These hybrid nanorods were synthesized by injecting 0 003 mmol $AuCl_3$ into 0.15 mmol as-synthesized CdSe nanorods solution. The average diameter of Au nanoparticles was 2 3 ± 0.7 nm
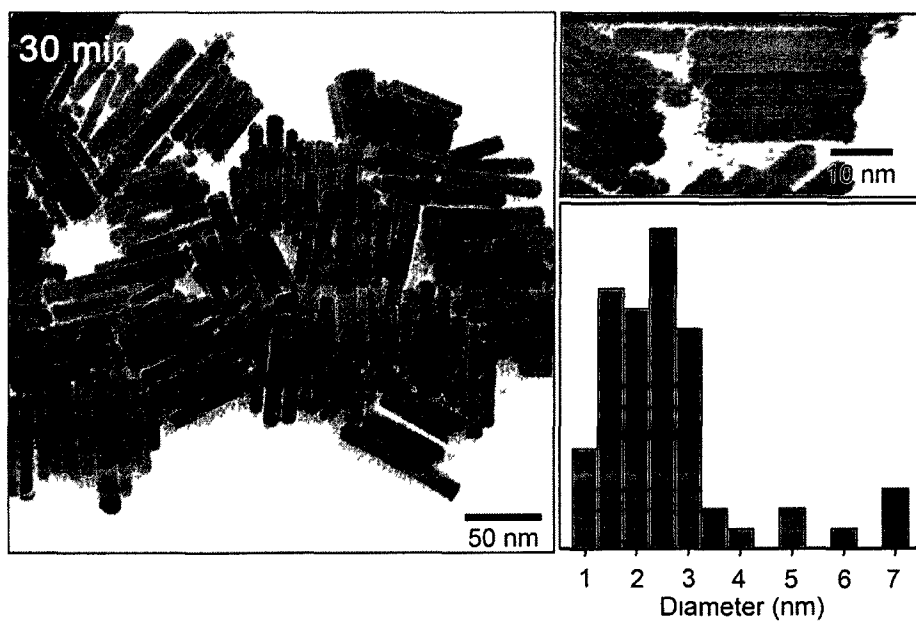
Figure 3.8 Original and enlarged TEM images of CdSe-Au hybrid nanorods and Au sizing histogram after 30 min reactions. These hybrid nanorods were synthesized by injecting 0 003 mmol $AuCl_3$ into 0 15 mmol as-synthesized CdSe nanorods solution. The average diameter of Au nanoparticles was 2.3 ± 1.3 nm

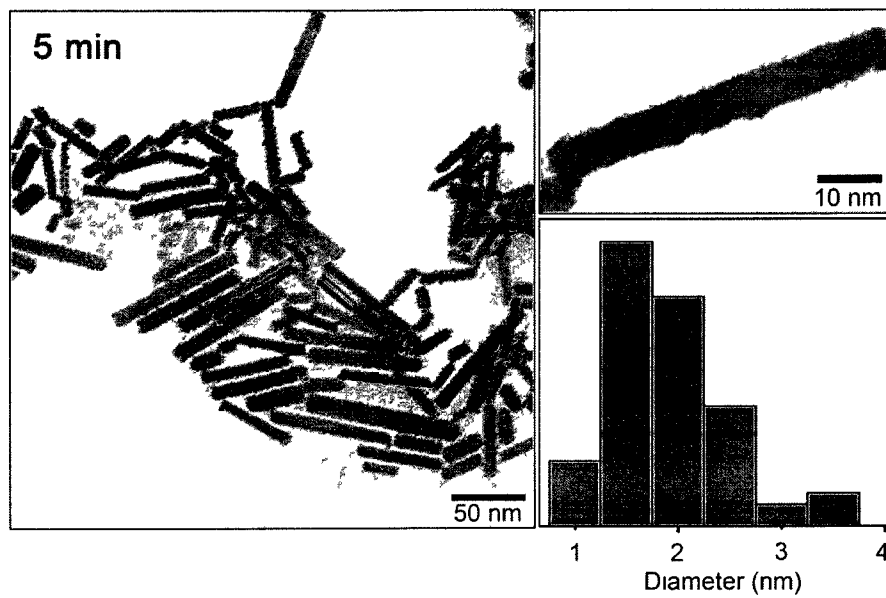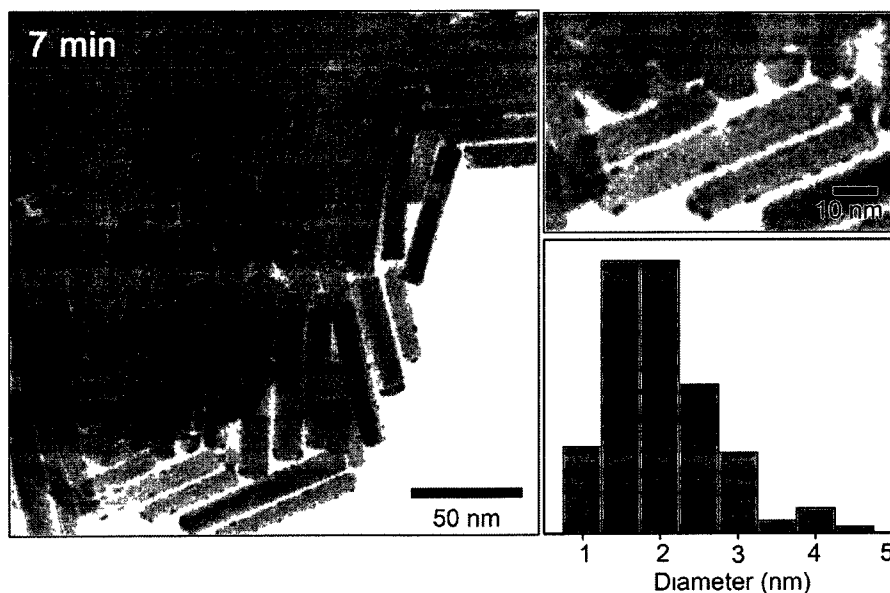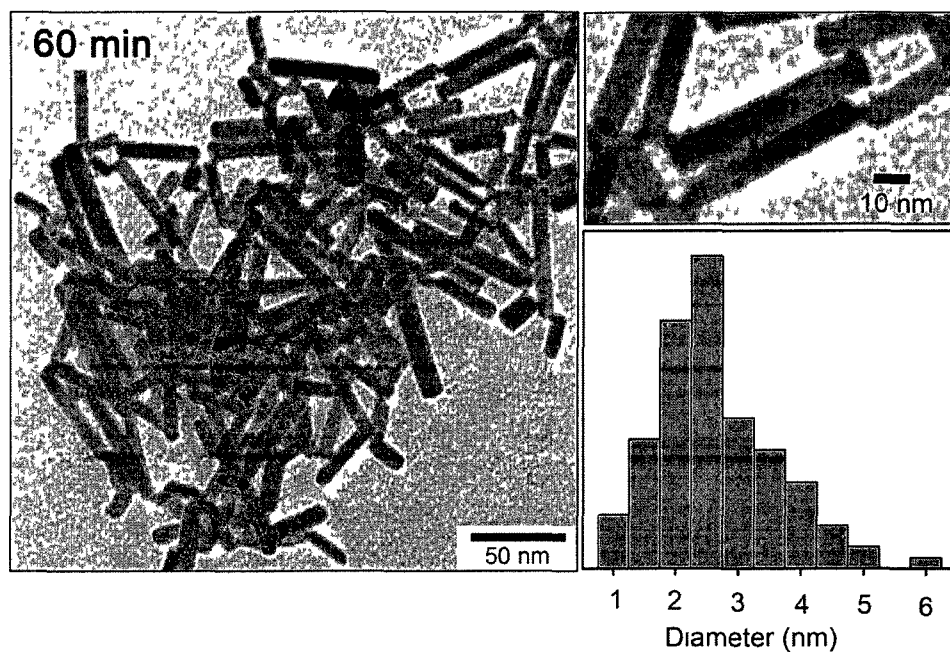**Figure 3.9** Original and enlarged TEM images of CdSe-Au hybrid nanorods and Au sizing histogram after 60 min reactions. These hybrid nanorods were synthesized by injecting 0.003 mmol $AuCl_3$ into 0.15 mmol as-synthesized CdSe nanorods solution. The average diameter of Au nanoparticles was 2.3 ± 0.9 nm.

The growth of Au nanoparticle on CdSe nanorods with respect to reaction time was shown in **Figure 3.10**. From the curve we can see that in the first 10 min, the average size of Au nanoparticles increased sharply from 0 to 2.3 ± 0.7 nm; after 10 min reaction, Au nanoparticles exhibited a rather stagnant growth: sizes changed from 2.3 ± 0.7 nm at 10 min to 2.4 ± 0.9 nm at 60 min. The time-dependent growth of Au nanoparticles can be attributed to the change of concentration of $AuCl_3$ in the solution at different reaction times. The formation of Au nanoparticles was triggered by the injection of $AuCl_3$. At the initial time point (t = 0), there was no Au nanoparticle observed. Once the $AuCl_3$ was injected into the solution, the reaction between Au^{3+} and Se^{2-} occurred subsequently at the surfaces of the CdSe nanorods. This reaction led to the formation of Au atoms on the

surfaces of CdSe nanorods. In the first 10 min, the Au nanoparticles kept growing at a relatively rapid growth rate due to the abundant $AuCl_3$ in the solution. As more Au nanoparticles formed in the solution, the concentration of Au^{3+} decreased until reaching the equilibrium. The growth rate of Au nanoparticles slowed down and ultimately suppressed by the depletion of the Au^{3+}, and the solution was considered to approach the equilibrium state. At an equilibrium state, the growth of Au nanoparticles transitioned to ripening state.

Figure 3.10 Changes of Au nanoparticles sizes as a function of reaction time

3.4.3 The Ostwald Ripening Process in CdSe-Au Solution

The Ostwald ripening process is the growth of large nanoparticles at the expense of dissolution of small ones at an equilibrium state. It is a spontaneous process because large nanoparticles are more thermodynamically stable than small ones. After the solution
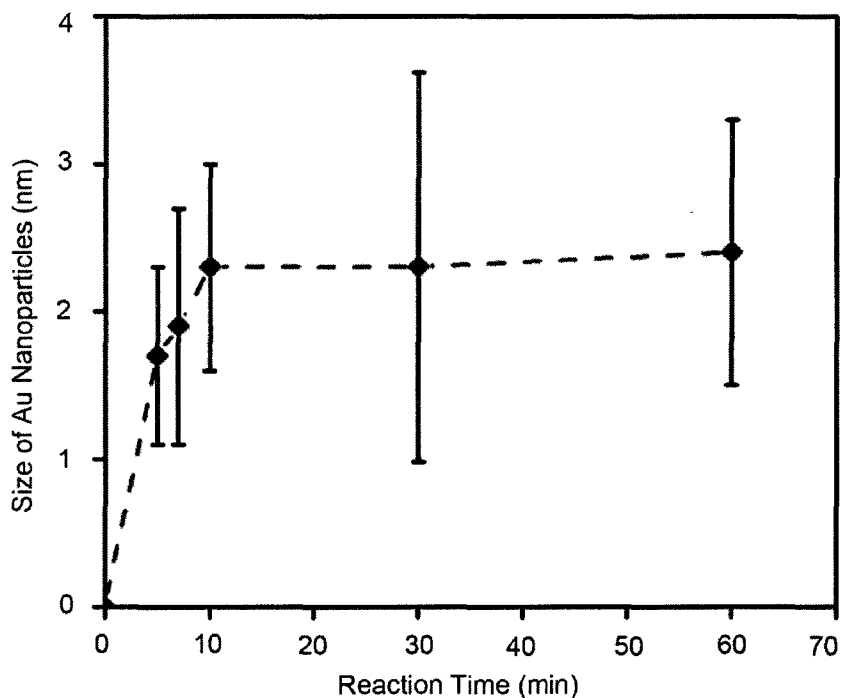
reached equilibrium state probably after 10 minutes reactions, large Au nanoparticles kept growing while small ones disappeared. Banin *et al.* first proposed a growth mechanism for this process that small Au nanoparticles first released electrons into solution and then transferred these electrons to large Au nanoparticles through CdSe nanorods [7]. After giving out electrons, the small Au nanoparticles escaped from the surfaces of nanorods and became free Au ions in the solution. These Au ions re-deposited on large Au nanoparticles and were reduced to Au^0 (**Figure 3.11**). The result of this process was disappearance of small Au nanoparticles and growth of large ones. However, they did not provide direct evidence to prove that small Au particles can release the electrons automatically. Also, no observation of electric current in CdSe nanorod was reported. Here, we proposed an alternative growth mechanism in which the growth of the Au nanoparticles is attributed to the Ostwald ripening process.
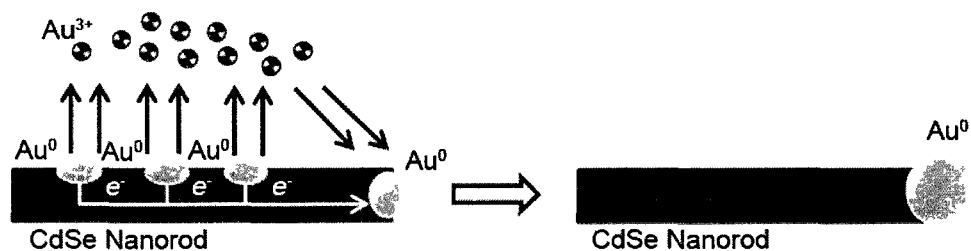
Figure 3.11 The growth process proposed by Banin *et al.* [2]. Small Au nanoparticles escape to the solution as free Au ions by release their electrons. The released electrons transfer to large Au nanoparticles to reduce Au ions in the solution and results in the growth of large Au nanoparticles.

From a standpoint of kinetics, when the concentration of $AuCl_3$ was high, formation of small Au nanoparticles was dominant. When Au atoms/clusters monomers were depleted, the whole system transited from a fast growth state (kinetics state) to a ripening

state (thermodynamics state). At the ripening state, from a standpoint of thermodynamics, small Au nanoparticles on the surfaces of CdSe nanorods dissolved into solution in the form of Au atoms (monomers) and re-deposited on the surfaces of large Au nanoparticles. As a result of this ripening process, the small Au nanoparticles dissolved to favor the growth of large particles on the CdSe nanorods. **Figure 3.12** shows the Ostwald ripening process in CdSe-Au hybrid nanorods solution at equilibrium state.
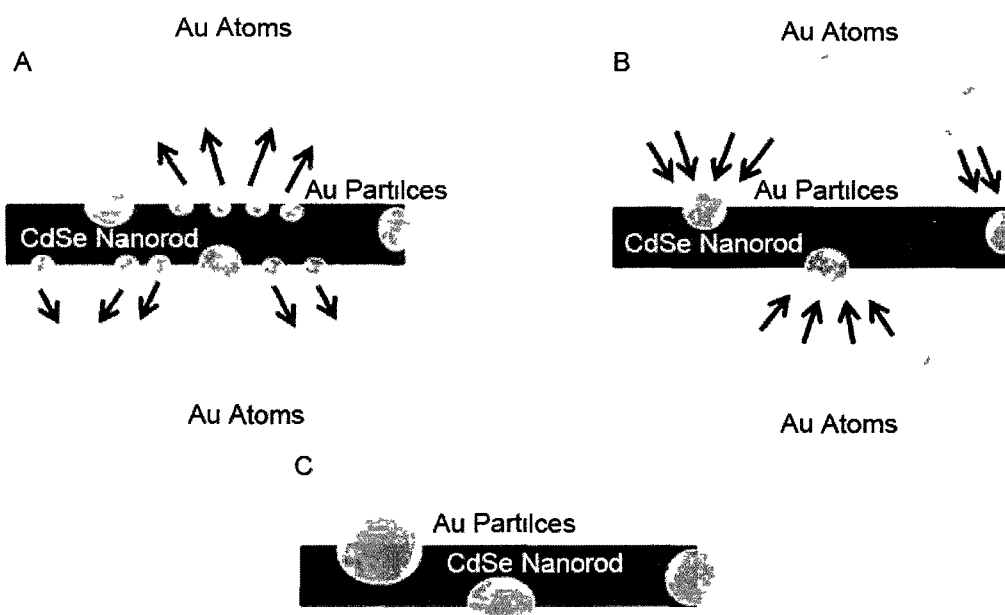
Figure 3.12 The Ostwald ripening process in CdSe-Au solution. (**A**) dissolution of small Au particles; (**B**) growth of large Au particles; (**C**) CdSe-Au hybrid nanorods with large Au particles.

As the reaction continued, we found that Au nanoparticles tend to migrate to the tips of CdSe nanorods. After 5 minutes reactions, (**Figure 3.5**), small Au nanoparticles were found all over the surfaces of CdSe nanorods. After 30 and 60 minutes reactions (**Figure 3.8** and **3.9**), Au nanoparticles were found mostly at the tips of CdSe nanorods. This migration of Au nanoparticles can be attributed to higher surface energies on the tips of nanorod, resulting from more accessible sites on the tips where surfactant capping was

weak. Therefore, the tips of nanorods are preferential growing sites for Au nanoparticles at long reaction times.

3.4.4 Elemental Analysis of CdSe-Au Nanorods

An elemental analysis using energy dispersive spectroscopy (EDS) was used to analyze the chemical composition of CdSe-Au. The samples of original CdSe nanorods and CdSe-Au hybrid nanorods after 7 minute reactions were measured as shown in **Figure 3.13** Cd and Se peaks could be observed clearly with no Au peaks in original CdSe nanorods. The appearance of Au peaks in CdSe-Au, together with the Cd and Se peaks, provided clear evidence that Au nanoparticles were formed. Also, the EDS results indicated that the atomic ratio between Se and Cd decreased to 1.2 in CdSe-Au sample comapred to that of 1.4 in the original CdSe nanorods. This is because during the galvanic replacement reaction process, Se^{2-} was consumed continuously by Au^{3+} while the amount of Cd^{2+} maintained at a constant value, which resulted in the decreasing of the atomic ratio between Se and Cd.
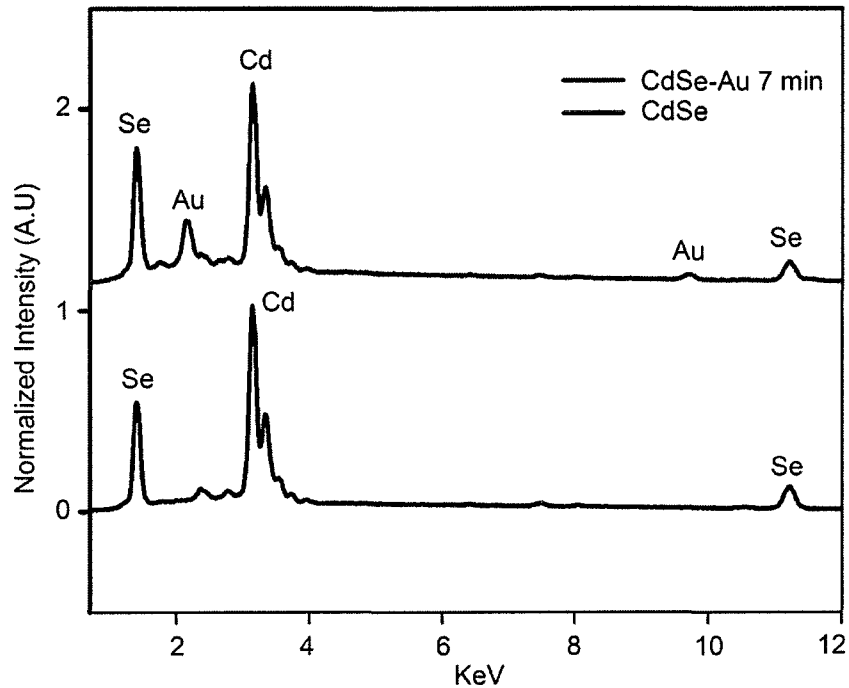
Figure 3.13 The EDS spectrums of original CdSe and 7 min CdSe-Au.

3.4.5 *In-Situ* Growth of Au Nanoparticles under Electron Irradiation in TEM

A unique growth of Au nanoparticles was observed under the irradiation of the electron beams in TEM. **Figure 3.14** shows this process. **Figure 3.14-A** is the original image of CdSe-Au nanorods after 7 min reactions exposed under electron beam of low intensity, Figure **3.14-B** is the same sample exposed under electron beam of high intensity for 1 min. From **Figure 3.14-A to B** we can see that as the electron beam intensity increased, the average size of Au nanoparticles experienced a clear growth from the initial 2.3 ± 0.7 nm to the final 5.0 ± 1.8 nm.
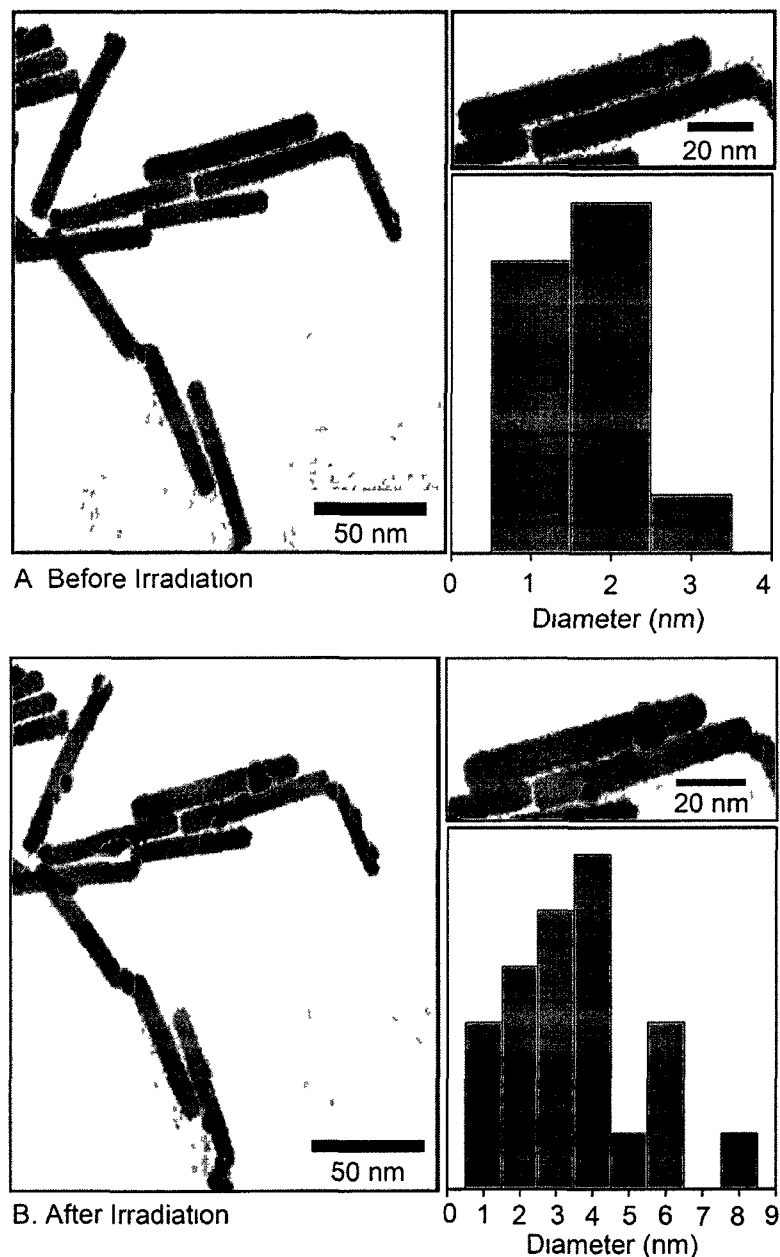
Figure 3.14 TEM images of CdSe-Au synthesized using 0.003 mmol AuCl₃ into 0.15 mmol CdSe nanorods: **(A)** before irradiation **(B)** after irradiation. The diameters of Au nanoparticles were **(A)** 2.3 ± 0.7 nm and **(B)** 5.0 ± 1.8 nm.

This unique growth of Au nanoparticles under electron irradiation can be attributed to the size effect on the melting point of Au nanoparticles. It has been approved that the melting points of nanoparticles have great dependencies to their sizes [9-11]. Typically, particles exhibit decreasing melting points with decreasing sizes. This size-dependent

melting point of nanoparticles can be calculated through the Gibbs-Thomson equation [11]:

$$T_M(d) = T_{MB}(1 - \frac{4\sigma_{sl}}{\rho_s d H_f})$$

where T_{MB} is bulk melting temperature, σ_{sl} is solid liquid interface energy, H_f is bulk heat of fusion, ρ_s is density of solids and d is particle diameter. From this equation we can see that as particle diameter d increases, the particle melting temperature $T_M(d)$ decreases. The melting point of bulk Au metal is 1336 k (1063 ℃). If the size of Au nanoparticle is 1.6 nm (the smallest Au nanoparticles we observed), the corresponding melting point is only 554 K (281 ℃) (The parameters for calculation are in **Table 3.3**). Also, the operation of TEM is under vacuum, which further decreases the melting points of small Au nanoparticles [12]. When Au nanoparticles were exposed to the electron beam in TEM, small Au nanoparticles melted easily due to their lower melting points. In the meantime, these melted Au particles were migrating towards large Au nanoparticles in order to achieve lower surface energies thermodynamically. The result of the process was the melting of small particles and the growth of large ones. The observed phenomenon also indicated that small Au nanoparticles distributed all over the surface of nanorod in the original sample. Otherwise, there were not enough growth resources for this dramatic growth of Au nanoparticles.

Table 3.3 Parameters for Calculating the Melting Point of Au Nanoparticle [9]

d/m	σ_{sl} /J m^{-2}	H_f/J Kg^{-1}	ρ_s/Kg m^{-3}	T_{MB}/K	$T_M(d)$/K	$T_M(d)$/ ℃
$1.6*10^{-9}$	0.27	$6.27*10^4$	$1.84*10^4$	1336	554	281

3.5 Conclusions

In summary, via the galvanic replacement reactions at room temperature, CdSe-Au hybrid nanorods with Au nanoparticles sizing from 1.7 ± 0.6 nm to 2.4 ± 0.9 nm were synthesized. We found longer reaction time yielded larger Au nanoparticles. During the growth process, $AuCl_3$ was reduced by Se^{2-} at the surfaces of CdSe nanorods to form Au nanoparticles. After the reaction was close to equilibrium state, the formed Au nanoparticles could keep growing and tend to migrate towards the tips of the CdSe nanorod to form larger ones in order to lower the surface energies. By using EDS, we analyzed the chemical compositions of CdSe-Au nanorods. An *in-situ* growth of Au nanoparticles under electron beam irradiation was observed. By studying the growth mechanism of this process, we confirmed that small Au nanoparticles distributed all over the surfaces of CdSe nanorods.

References:

1. Y. Yamamoto, T. Miura, M. Suzuki, N. Kawamura, H. Miyagawa, T. Nakamura, K. Kobayashi, T. Teranishi, and H. Hori, Diameter dependence of ferromagnetic spin moment in Au nanocrystals, *Phys. Rev. B.* **69**. 174411 (2004).

2. Y. Yamamoto, T. Miura, M. Suzuki, N. Kawamura, H. Miyagawa, T. Nakamura, K. Kobayashi, T. Teranishi and H. Hori1, Direct Observation of Ferromagnetic Spin Polarization in Gold Nanoparticles, *Phys. Rev. Lett.* **93**. 116801 (2004).

3. P. Crespo, R. Litran, M. Multigner, J.M. de la Fuente, J.C. Sanchez Lopez, M.A. Garcia, C. Lopez Cartes, A. Hernando, S. Penades, A. Fernandez, Permanent magnetism, magnetic anisotropy, and hysteresis of thiol-capped gold nanoparticles, *Phys. ReV. Lett.* **93**, 087204 (2004).

4. A. Hernando, P. Crespo, M.A. Garci´a, E. Ferna´ndez Pinel, J.de la Venta, A. Ferna´ndez, S. Penade´s, Giant magnetic anisotropy at the nanoscale: Overcoming the superparamagnetic limit, *Phys. ReV. B*, **74**, 052403 (2006).

5. T. Mokari, E. Rothenberg, I. Popov, R. Costi and U. Banin, Selective Growth of Metal Tips onto Semiconductor Quantum Rods and Tetrapods, *Science*. **304**, 1787-1789 (2004).

6. G. Menagen, J. E. Macdonald, Y. Shemesh, I. Popov and U. Banin, Au Growth on Semiconductor Nanorods: Photoinduced versus Thermal Growth Mechanisms, *J. Am. Chem. Soc.* **131**, 17406–17411 (2009).

7. T. Mokari1, C. G. Sztrum, A. Salant, E. Rabani and Uri Banin, Formation of asymmetric one-sided metal-tipped semiconductor nanocrystal dots and rods, *Nature Mater*, **4**, 855-863 (2005).

8. A. E. Saunders, I. Popov and U. Banin, Synthesis of hybrid CdS-Au colloidal nanostructures, *J. Phys. Chem. B.* **110**, 25421-25429 (2006).

9. P. Buffat and J. P. Borel, Size effect on melting temperature of gold particles, *Phys. Rev. A.* **13**. 2287 (1976).

10. M. Takagi, Electron-diffraction study of liquid-solid transition of thin metal films, *J. Phys. Soc. Jpn.* **9**, 359-363 (1954).

11. J. Sun and S. L, Simon, The melting behavior of aluminum nanoparticles, *Thermochimica Acta*, **32**, 463 (2007).

12. GL. Allen, RA. Bayles, W. Gile, WA. Jesser, Small particle melting of pure metals, *Thin Solid Films,* **144**, 297 (1986).

13. www.webelements.com

CHAPTER 4 CONCLUSIONS AND FUTURE WORK

The target of this work was to synthesize CdSe-Au hybrid nanorods. The first step was to synthesize CdSe nanorods. A simple mono-injection method was adopted in the syntheses. By reducing the molar ratios between Se and Cd, we have successfully achieved the shape control of CdSe nanocrystals from nanoparticles to nanorods. We found 5 to1 was a critical molar ratio between Se and Cd to form different CdSe nanostructures. When the molar ratio between Se and Cd was higher than 5 (6.7), CdSe nanoparticles were synthesized. When the molar ratio was lower than 5 (1.2 and 1.7), CdSe nanorods were synthesized. The growth models for different CdSe nanostructures were proposed and validated by the subsequent experimental results. In the model, the concentration of monomer plays an important role in the shape control of CdSe nanostructures. High concentration of monomer leads to the isotropic growth of CdSe nanoparticles. Low concentration of monomer leads to the anisotropic growth of CdSe nanorods. Comparing with traditional approach adopted in the shape control of CdSe nanostructures, the synthesis approach used in this work is more easy to conduct; also a relatively moderate reaction temperature and more favorable Cd precursor make the synthesis approach safer.

The growth of Au nanoparticles on CdSe nanorods involves galvanic replacement reactions between $AuCl_3$ and CdSe nanorods at room temperature. In the reaction, Au^{3+} was reduced to Au atoms while Se^{2-} was oxidized to Se^{4+}. By adjusting the reaction times, Au nanoparticles with diameter from 1.7 ± 0.6 nm to 2.4 ± 0.9 nm could be synthesized

on the surfaces of CdSe nanorods. Before the reaction closing to equilibrium state, Au nanoparticles exhibited a fast growth rate due to a high concentration of $AuCl_3$ in solution. When the concentration of $AuCl_3$ approaching to equilibrium level, the reaction was closely related to the Ostwald ripening process in which the small Au nanoparticles dissolved into solution and the mass was transferred to increase the size of the large nanoparticle on the nanorods. According to the previous literature, Au nanoparticles with diameter less than 3 nm displayed ferromagnetism even at room temperature [1, 2]. Hence, the additional work to test the magnetic properties of these CdSe-Au hybrid nanorods would be necessary in the future work. If the ferromagnetism of CdSe-Au hybrid nanorod system can be observed at room temperature, it will provide strong scientific basis to the development of DMS.

References:

1. P. Crespo, R. Litran, M. Multigner, J.M. de la Fuente, J.C. Sanchez Lopez, M.A. Garcia, C. Lopez Cartes, A. Hernando, S. Penades, A. Fernandez, Permanent magnetism, magnetic anisotropy, and hysteresis of thiol-capped gold nanoparticles, *Phys. ReV. Lett.* **93**, 087204 (2004).

2. A. Hernando, P. Crespo, M.A. Garcı́a, E. Fernández Pinel, J.de la Venta, A. Fernández, S. Penadés, Giant magnetic anisotropy at the nanoscale: Overcoming the superparamagnetic limit, *Phys. ReV. B*, **74**, 052403 (2006).